ptt to Sullivan

BELLCOMM INC.

BELL SYSTEM

GPO PRICE $ _____

CFSTI PRICE(S) $ _____

Hard copy (HC) 3.00

Microfiche (MF) .75

ff 653 July 65

FACILITY FORM 602

N66-12857
(ACCESSION NUMBER)

69
(PAGES)

CR-68189
(NASA CR OR TMX OR AD NUMBER)

1
(THRU)

(CODE)

30
(CATEGORY)

NC-64-02-20-MEP

THE METEOROID ENVIRONMENT OF PROJECT APOLLO

Edition 2

Revised, February 20, 1964

G. T. Orrok

Bellcomm, Inc.
Washington, D. C.

TABLE OF CONTENTS

PURPOSE AND SCOPE

To discuss the meteoroid hazard to the currently conceived Apollo mission, a knowledge of three factors is required.

These are (1) the potential hazard offered by the environment, (2) the susceptibility of the spacecraft as indicated by its detailed design, and (3) the allowable hazard, as governed by considerations of over-all system reliability.

The scope of this document is restricted to the first factor.

ABSTRACT

12857

The meteoroid environment of the Apollo mission is reviewed. A model for engineering design purposes is presented. The principal inputs are the Explorer XVI penetration data, the flux mass relations for visual and radar meteors, and a modified Ames penetration equation. The zero magnitude meteor of velocity 30 km/second has a mass of one gram and a density of one gram per cc. After analysis of available data, it is estimated that the solid skin thickness required for protection to a given impact probability is known to a factor of about 2.1 times.

Erosion rates as estimated from Explorer XVI data are negligible. The variation of penetration hazard among low earth orbit, deep space, and the lunar surface is thought small.

Author

PREFACE TO THE SECOND EDITION

In the first edition of "The Meteoroid Environment of Project Apollo", revisions were promised "as more experimental facts become available." Very considerable progress has been made and it seems appropriate to up-date the document at this time.

New topics to be discussed are the Explorer XVI results, and some preliminary publications of the Harvard Radio Meteor program. Professor Whipple's most recent meteoroid model is discussed in an appendix, as is the proposed SA-9 experiment. The sections dealing with the nature of dust balls, hypervelocity impact measurements, and the hazards in deep space and the lunar surface are expanded or substantially altered. A new "best estimate for engineering purposes" will be presented.

Despite the increase in subtlety and in volume, the information directly pertinent to the puncture of the Apollo spacecraft has not improved much in accuracy. The uncertainties in luminous efficiency, meteoroid composition and structure, and in the penetration law have not been substantially reduced. Furthermore, the nominal puncture probabilities have not changed significantly, a number of small changes having compensated each other.

As in the first edition, the text is directed towards the development of the "model", and more detailed studies appear in the appendices. The references are listed alphabetically, and a table of symbols is included as Appendix 1.

THE METEOROID ENVIRONMENT OF PROJECT APOLLO

SECOND EDITION

1.0 INTRODUCTION

The Apollo spacecraft will encounter large numbers of meteoroids on its lunar landing mission. The vast majority of the particles are small, and are not dangerous as far as puncture is concerned. On the other hand, larger meteoroids (on the order of a kilogram) are so infrequent as to be negligible. The particles of real concern have diameters under a millimeter, and weights in the milligram range. The velocities of these specks are characteristic of any bodies in orbit around the sun. They range (entering the earth's atmosphere) from 10 to 70 km/sec. The kinetic energy per unit mass far exceeds the yield of TNT.

Enhanced or reduced hazards occur where either the mass or velocity distribution of the particles is affected. Near a planetary mass the particle velocities are increased. Meteoroid streams or showers follow narrowly defined orbits around the sun. Depending on the population of the particular shower, substantial increases in hazard are possible when the spacecraft intercepts such an orbit. On the earth's surface, the atmosphere reduces the hazard to nil.

Other inhomogeneities in the meteoroid distribution today seem less important. Though a large number of smaller particles may be in orbit around the earth, they do not present a hazard. On the moon's surface, each primary meteoroid impact will generate quantities of secondary particles of low velocity; quantitative current estimates suggest strongly that these are not dangerous.

The hazard to a given space flight may be described by two numbers: firstly, a probability of puncture; and secondly, a depth or degree of surface erosion. It appears that the erosion hazard is very small.

The puncture probability is proportional to the "exposure" of the spacecraft, defined as the product of its area by the time it spends in a region of homogeneous danger. The units of exposure are chosen as square meters seconds.

The exposure of the Apollo mission sets narrow limits on the meteoroid fluxes of interest. For an order of magnitude estimate of these limits, we assume the Apollo area to be 70 square meters, and the length of the mission to be 14 days. The exposure is about $10^8 m^2 sec$. The wall thicknesses range from one half to five millimeters of single aluminum wall.

Suppose we are concerned with a structural wall equivalent (as far as penetration is concerned) to T meters

of aluminum. The penetrating flux, N(T), is defined as the mean number of meteoroids impacting this wall per square meter, per second, per 2π steradians (i.e., from one side) capable of penetrating T or more meters of aluminum. This is a cumulative, omnidirectional, flux, including all particles with greater penetrating power. Spacecraft in low earth orbit are "shielded" below by the earth. Dr. Whipple (63) quotes a "near earth flux" which is automatically smaller by a half than that used here.

For a given thickness and mission exposure, E, the mean impact rate is E N(T).

If E N is less than a tenth, this is nearly the probability of one impact, P_1, and, approximately,

$$P_1 \sim E\,N(T)\,, \quad E\,N(T) \ll 1. \tag{1.1}$$

The "significant" meteoroid fluxes for Apollo design are those which are expected to impact infrequently -- that is, the skin must be proportioned to withstand those particles which impact only once in many missions. Then P_1 is perhaps 10^{-1} to 10^{-3}. With an exposure of $10^8 m^2 sec$, the "significant flux range" becomes

$$\underline{\text{Significant flux for Apollo:}} \quad 10^{-11} < N(T) < 10^{-9}\ m^{-2}\ sec^{-1} \tag{1.2}$$

The primary objective of a meteoroid environment model for Project Apollo is to describe the properties, including the skin just penetrated, of particles having these fluxes.

In addition, the environment model should describe the "significant fluxes" for a suited astronaut. We may assume him to have an area of 2 square meters exposed for one day, or an exposure of $10^5 m^2 sec$. The significant fluxes are, by the same reasoning,

$$\underline{\text{Significant flux for astronaut:}} \quad 10^{-8} < N(T) < 10^{-6} \tag{1.3}$$

Proof tests to determine the relative puncture resistance of aluminum and multi-layer fabrics like those proposed for the Apollo suit are in progress.

Finally, the environment should describe the degree of erosion expected on an Apollo mission. Penetration information can be converted into an expectation of cratering on thick targets. The significant fluxes for erosion are those of the most numerous particles.

In this document, the puncture environment for spacecraft and astronaut will be emphasized. A section on erosion concludes the text.

Let us consider the sources of information on meteoroid penetration rates. The most useful information for Apollo would be obtained from penetrations measured in engineering structures, or penetration depths measured on recovered vehicles. To be optimum, however, the structures should exceed a millimeter in thickness, and the experimental exposure should be many times that of Apollo. The scheduled Saturn-launched micrometeoroid measurement capsules (SA-9, SA-8)(see Appendix 7) offer good exposure ($10^{10} m^2 sec$) but are somewhat thin (0.4 mm). To compensate, the thin experiments (for given exposure) have high counting rates and may define variations of the puncture flux with space and time.

The currently available information includes penetration measurements made in a flux range higher than the one of direct relevance to the Apollo spacecraft, and indirect measurements (meteor data) requiring much interpretation.

The very valuable results from Explorer XVI define the near-earth puncture rate down to a flux of about 5×10^{-7} and up to a thickness of about 0.2 mm of equivalent aluminum. In this range, the meteoroid hazard is less than was generally anticipated. For instance, the puncture rate of 1 mil beryllium copper is thirty times less than the nominal estimate in the first edition of this paper, which was based principally on the indirect, meteor data. The discrepancy is not far beyond the "expected error" of that estimate; however, the relative puncture rates in one and two mil beryllium copper are inconsistent with the older estimate. A straight line extrapolation of the Explorer XVI results to the "significant range" for Apollo exceeds the old estimate there.

The other data are in the form of particle fluxes measured as a function of impact momentum, meteor brightness, and meteor trail ionization. Only the latter are in the significant range. To be useful, these data require considerable interpretation. They must be combined with laboratory estimates of penetration which are themselves discordant. The interpretation is difficult. We disagree strongly, for instance, with Dr. F. W. Whipple on several aspects of his recent meteoroid model (Whipple 63).

In the following pages these data are reviewed. An attempt is made to produce a best estimate of hazard rates, together with an estimate of confidence. The error interval is wide; the appraisal is subject to revision as more experimental facts become available.

2.0 METEOROIDS: GENERAL

This section is concerned with qualitative description and definitions. For a broader background, the reader is advised to read McKinley (1961) or, for a splendid semitechnical account, Watson (1956).

A meteoroid is a small object in space. Upon entering the earth's atmosphere, it is consumed, emitting light -- in short, it becomes a meteor. Heavier objects may reach the ground. These may be recovered as meteorites. Lighter objects too faint to be seen may generate enough ionization to be detected by radar as radio meteors. Micrometeoroids are particles sufficiently small that the heat generated in passing through the atmosphere can be radiated away without the consumption of the body. The resulting micrometeorites may be collected (as magnetic dust particles) on earth.

The meteoroids fall into two families characterized by orbit as asteroidal and cometary particles. Mechanical strength and other properties correlate with this distinction.

2.1 Asteroidal Meteoroids

The asteroidal particles enter the atmosphere and are consumed as single bodies. The rate of light generation obeys "single body" theory. The family includes at least the smaller meteorites. It is therefore possible to infer that most asteroidal meteors are "stone" of density approximately 3 grams per cc, with a few "irons" of density about 8 gm/cc. The most brilliant meteors (brighter than visual magnitude -5) are predominantly asteroidal.

In the range significant to Apollo, asteroidal meteors occur if at all only once in a hundred to a thousand instances. We may therefore safely ignore the asteroidal contribution to the meteoroid hazard. As a purely speculative point, however, measurements by earth satellites indicate that there may be two fluxes of meteoroids: one causes microphone impulses and the other, smaller by a thousand times, is capable of penetration. This empirical distinction will be used below.

2.2 Cometary Meteoroids

The second family, the cometary meteoroids, are predominant among the fainter visual and the radio meteors. Not only are their orbits similar to those of comets, but they often are localized in a known comet orbit. These groups are the meteor showers.

Cometary meteoroids are very fragile. As clearly indicated by both photographic and radar techniques, they fragment into tiny pieces high in the earth's atmosphere. Opik (1958) computed typical numbers of fragments (for visual meteors) of 10 to 100, and for the Draconid shower of 1946, 10^6. Hawkins and Southworth (1963) report that radio meteors average approximately 4000 fragments, and that the breakup occurs sooner and more completely than it does for the visual meteoroids. The approximate dynamic pressure causing disruption is estimated as 1/3 psi, a material strength comparable with cigar ash.

The measured quantities which characterize meteors are vector velocity, deceleration, light intensity (visual meteors) and trail electron density. Integrals of the last two quantities are used to derive mass. There are no spectra of meteors fainter than magnitude zero, and thus, no estimates at all of composition. It will appear that the mass of a meteor can be estimated with reasonable accuracy only if chemical composition is well known.

The deceleration measurement has in the past been used to derive a meteoroid density. In fact, it yields a measure of the ratio of mass to frontal area for the individual decelerating particles -- the fragments of a dust ball.

There is no information as to the structure of the complete particle in space, save that it is fragile. These facts are very important. They set fundamental limitations on the accuracy of hazard estimates from this source.

2.3 Space Distribution: The Showers

Perhaps a quarter of visual meteors belong to major showers, in which fluxes may considerably exceed the average, or sporadic, flux. Five times is characteristic for a strong yearly shower, such as the Perseids, in which the meteoroids are spaced fairly uniformly around their orbit. An increase of a thousand times may occur for periodic showers, whose particles are localized within the orbit. The duration of intense showers can be extremely brief (1-5 hours). Unless the earth's year and the shower period are simply related, long intervals may separate recurrences of periodic showers.

It should be emphasized that showers differ. The predominant mass of meteor differs; the mean number of fragments per particle differs; for many showers, the flux increase in the radar meteor range is much less than that in the visible. Considerable work needs to be done before showers can be quantitatively included in a model.

Appendix 2 is a table taken largely from McKinley (1961). It shows the names and dates of major showers, their radiants (apparent origin in the celestial sphere), velocities, and an indication of relative rates expected. It should be noted that there are months -- February and September -- without major showers.

3.0 PENETRATION CRITERION

The quantity of immediate interest to Apollo is the flux of meteoroids capable of penetrating a given structural skin. A criterion must be chosen which within some error permits the conversion of data to puncture rates in a reference skin configuration and, conversely, the prediction from this reference configuration of puncture rates in engineering structures.

No proposed criterion has adequate theoretical justification; all fit some sub-set of the available data fairly well. In this document we use a modification of the Ames (Summers 1959) penetration criterion. It more than adequately represents the understanding of current experimental data.

The reference skin is a single aluminum wall of unspecified strength. The additional impact resistance of a "hard" alloy decreases with projectile velocity, and may be illusory for meteoroid impacts. A "soft" alloy is, at the conclusion of cratering, heavily cold worked, so that measurements made before the impact should be misleading.

3.1 Hypervelocity Impact

The results of hypervelocity impact in a thick target can be briefly described. By "hypervelocity" we mean that the projectile velocity exceeds the speed of sound in the target. This is about 5 km/sec in most structural metals. Meteoric speeds relative to spacecraft may range from zero to 70 km/second, averaging about thirty.

The experimental data on hypervelocity impact (as reported for instance in the Sixth Symposium on Hypervelocity Impact (HIS, 1963)) is excellent to velocities of 6 km/sec, good to 10 km/sec, and sparse above that velocity. The indications are that crater volume far exceeds projectile volume, that the elastic and plastic constants of the substrate to some degree control crater size, that the craters are nearly hemispherical, but that particle density and aspect ratio control the precise shape.

3.2 Impact Model: Cratering in Deep Targets

In the first edition of this document we used the Charters and Locke (1958) penetration equation. As refined by Summers (1959), this is:

$$\frac{p}{d} = 2.28 \left(\frac{\rho_p}{\rho_t}\right)^{2/3} \left(\frac{v}{c}\right)^{2/3} \qquad (3.1)$$

where p is the crater depth, d is the diameter of a spherical projectile, ρ_p and ρ_t are the densities of particle and target, v is the normal component of projectile velocity, and c the speed of sound in the target. For irregular particles the dimension d to be used is that measured along the line of flight.

The Ames correlation for crater volume, V_T, versus particle volume, V_P, does not show the density dependence one would expect if the craters were hemispherical. Cubing equation (3.1), one would obtain a factor $(\rho_p/\rho_t)^2$, but instead one finds

$$\frac{V_T}{V_P} = 34 \left(\frac{\rho_p}{\rho_t}\right)^{3/2} \left(\frac{v}{c}\right)^2 \qquad (3.2)$$

This may be interpreted as a crater shape effect. If one assumes ellipsoidal craters of depth p and diameter D_c, and combines equations (3.1) and (3.2), one obtains

$$\frac{p}{D_c} = 0.58 \left(\frac{\rho_p}{\rho_t}\right)^{1/4} \qquad (3.3)$$

This shape factor appears a valid fit to measured data at velocities of 6-9 km/sec. There is no trend of increasing sphericity. Charters (HIS 63) quotes equations similar to (3.1) and (3.2) obtained for impacts on aluminum at 6 km/sec. Although the density dependences are quite dissimilar, equation (3.3) survives unchanged.

It appears that penetration (3.1) rather than volume equations should be used.

We rewrite (3.1) in terms of particle mass. Remembering that the dimension, d, is that along the line of flight, we assume the particle an ellipsoid of revolution with axial length d and aspect ratio A. The particle mass is

$$m_p = \frac{\pi \rho_p d^3}{6 A^2} \qquad (3.4)$$

Now, equation (3.1) becomes

$$p = 2.8 \left(\frac{\rho_p}{\rho_t}\right)^{1/3} A^{2/3} \left(\frac{m_p v^2}{\rho_t c^2}\right)^{1/3} \qquad (3.5)$$

The functional dependence on particle and target properties will be discussed below. For application to meteoroid impact, certain modifications must be made. In

particular, it appears that target strength should be included as a parameter. It is not clear how this should be done.

3.2.1 Dependence on Target Strength

Target strength appears in equation (3.5) as a factor $(\rho_t c^2)^{-1/3}$. The empirical data reflect a dependence on material condition -- that is, a work hardened or heat treated specimen of high strength is more resistant to cratering than an annealed specimen. This is not entirely unreasonable, since the cratering action will continue until the stresses are less than the material strength. The strength in question is not that of the target as evaluated prior to impact, but that after exposure to high pressures.

A number of penetration criteria correlate penetration with the Brinnell Hardness Number, H, of the target. The scatter in the data is wide, but the following statements may be made.

(a) Penetration at low velocities may be scaled by $(H)^{-1/3}$, although this dependence appears too strong for materials of very high or low strength.

(b) For many materials of ordinary strength $(\rho_t c^2)^{-1/3}$ scaling (used here) gives comparable results. If Y is the appropriate elastic constant, $\rho c^2 = Y$.

(c) At high velocities, the dependence on H weakens. Bjork (HIS 63) suggests that $(H)^{-0.15}$ is a suitable relation. The body of data at high velocities seems consistent with this. The modest success of (ρ, c) scaling is unimpaired.

In choosing the Ames criterion, with (ρ, c) scaling, we are asserting that at meteoric velocities the dependence of penetration on material strength will be substantially less than in the empirical range. It is to be hoped that further hypervelocity impact work will clear up this situation.

3.2.2 Dependence of Equation (3.5) on Particle Velocity

The velocity dependence of penetration is discussed at length in Appendix 3. The hypervelocity data is falling away from a $v^{2/3}$ law, and we make our only modification of the Ames equation here, dropping to a $v^{1/2}$ dependence above 10 km/sec.

3.2.3 Dependence of Equation (3.5) on Angle of Incidence

The Ames criterion states that penetration is a function of the normal component of projectile velocity.

The empirical data is contradictory, but no dependence stronger than (v cos Θ) has been proposed.

3.2.4 Dependence of Equation (3.5) on Projectile Density

This is discussed in Appendix 3. Briefly, a review of the literature suggests that the dependence used here, $(\rho_p)^{1/3}$, is valid in the lower empirical range (to 3 km/sec), and is an upper bound at higher velocities.

3.2.5 Dependence of Equation (3.5) on Aspect Ratio

Equation (3.5) depends on $A^{2/3}$. Since the value A = 1 will be used in the model environment, this does not require detailed criticism; there is little doubt that it is too strong.

3.2.6 General Comments

Any dependence of crater size and shape on particle strength, density, aspect ratio, and perhaps angle of incidence can be regarded as "information" about the initial condition of the impact which propagates with the shock wave and appears in the resulting crater. One may infer that if the crater is much larger in size than the projectile (as it is at high velocity), the transmission of this information will be weakened. The projectile "dimension" here would have to be a maximum dimension; in the case of angle of incidence, one might use the distance traveled tangent to the surface before the particle is entirely engulfed by the impact shock. For large craters, then, the dependences on particle properties in equation (3.5) are likely to be reduced. Then, if we have perhaps overestimated penetration by ignoring target strength, we have possibly obtained a balance by somewhat overestimating the ameliorative effects of angle of incidence and meteoroid density. It is our opinion that for this particular application the modified Ames equation is well chosen. It appears as

$$p = 2.8 \left(\frac{\rho_p \, m_p \, 10^2}{\rho_t^{2/3} \, c^{1/2}} \right)^{1/3} \left(\frac{v \cos \Theta}{c} \right)^{1/2} \qquad (3.6)$$

The modifications are that A = 1 and that, above 10 km/sec, p varies as $v^{1/2}$.

3.3 Impact Damage

Having chosen a standard equation for estimating crater depths, we must relate this to damage of practical

walls of various types. The following numerical instances represent general opinion (HIS 63).

(a) A projectile which makes a crater p_1 units deep in one material will make a crater p_2 units deep in another. If possible, good experimental data based on impacts at velocities well above 5 km/second should be used. Otherwise

$$p_2 = p_1 \left(\frac{c_1 \rho_1}{c_2 \rho_2} \right)^{2/3} \tag{3.7}$$

may be used.

(b) A projectile which makes a crater p units deep in a thick material will penetrate a wall 1.8 p in thickness. The number 1.5 was used in the first edition, but various authors (HIS 63) mentioned experimental values between 1.5 and 2.

(c) A projectile which makes a crater p units deep in a thick material may cause spallation from the rear surface of a wall 2.3 p in depth.

(d) Suppose a projectile will just penetrate a wall of thickness T. One may use instead of a single wall a meteoroid bumper. The meteoroid is fragmented by impacting the outer sheet. A rather thinner total structure, T_1, is then permissible. The advantage is represented by a bumper factor, $B = T/T_1$. Bumper factors of 1.5 are usually assumed, although factors as high as 4 have been proposed for special, widely spaced structures. Continuation of current experimental and theoretical studies (for instance, Maiden (HIS 63)) should lead to a reasonable understanding of the capability of bumpers.

3.4 Penetration Model

We now express the wall thickness, T, which can just be punctured. From equation (3.6) we obtain,

$$T = 5.09 \left(\frac{\rho_p \, m_p}{\rho_t^{\,2}} \left(\frac{10^4}{c} \right)^2 \right)^{1/3} \left(\frac{v \cos \theta}{10^4} \right)^{1/2} \tag{3.8}$$

The "standard wall" is taken as aluminum of $\rho_t = 2.7 \times 10^3 \text{kg/m}^3$ and $c = 0.51 \times 10^4 \text{m/sec}$. Equation (3.8) becomes:

$$T = 0.41 \left(\frac{\rho_p \, m_p}{10^3} \right)^{1/3} \left(\frac{v \cos \theta}{10^4} \right)^{1/2} \tag{3.9}$$

4.0 PENETRATING FLUX: MEASURED: EXPLORER XVI

Since the numerical quantity of immediate interest to Apollo is the flux of particles penetrating a structural skin, the direct measurements on the satellite Explorer XVI are of great importance. The measured fluxes fall just above the significant range for suited astronauts, but far from the significant flux for the Apollo spacecraft.

Two of the experiments are of particular interest in the sense that they define both a flux level and a size dependence. These are the pressurized can experiment and the cadmium sulfide cell experiment.

4.1 Pressurized Can Experiment

More than half of the surface of Explorer XVI was covered with pressurized cans fabricated from beryllium copper of various thicknesses. Puncture of the can resulted in operation of a pressure switch, which was then both a detector and a memory element. By the end of July, of the 100 cells of .001 inch beryllium copper, 44 were punctured, 11 of the 40 .002 inch cells were punctured, and none of the 20 .005 inch cells were punctured.

A preliminary report has been circulated within NASA (Hastings 1963), including an excellent statistical treatment of the data through May 26. (Explorer XVI was launched December 16 and operated without malfunction through about the first of May. Most of the experiment was functioning until the end of July.) The results are reviewed in Appendix 4. The fluxes (as of May 26) are plotted as 90% confidence intervals on Figure 1. The "equivalent thickness of aluminum" is twice that of beryllium copper, as determined by impact experiments at about 5 km/second.

4.2 Cadmium Sulfide Cell Experiment

Two cadmium sulfide cells were flown on Explorer XVI. Punctures in an aluminized quarter mil mylar film allowed sunlight to illuminate the photoconductive cells periodically, as the satellite tumbled. The telemetered minimum cell resistance is a measure of the total open area. Although the total exposure of this experiment is smaller than that of one pressurized can, the data complement the beryllium copper data well. The number of area changes recorded is a measure of flux; the distribution of areas is a measure of the size distribution; finally, the values of the areas should give information about the nature of the penetrating particle.

Some preliminary data on the results of this experiment have been kindly communicated to us by L. Secretan.

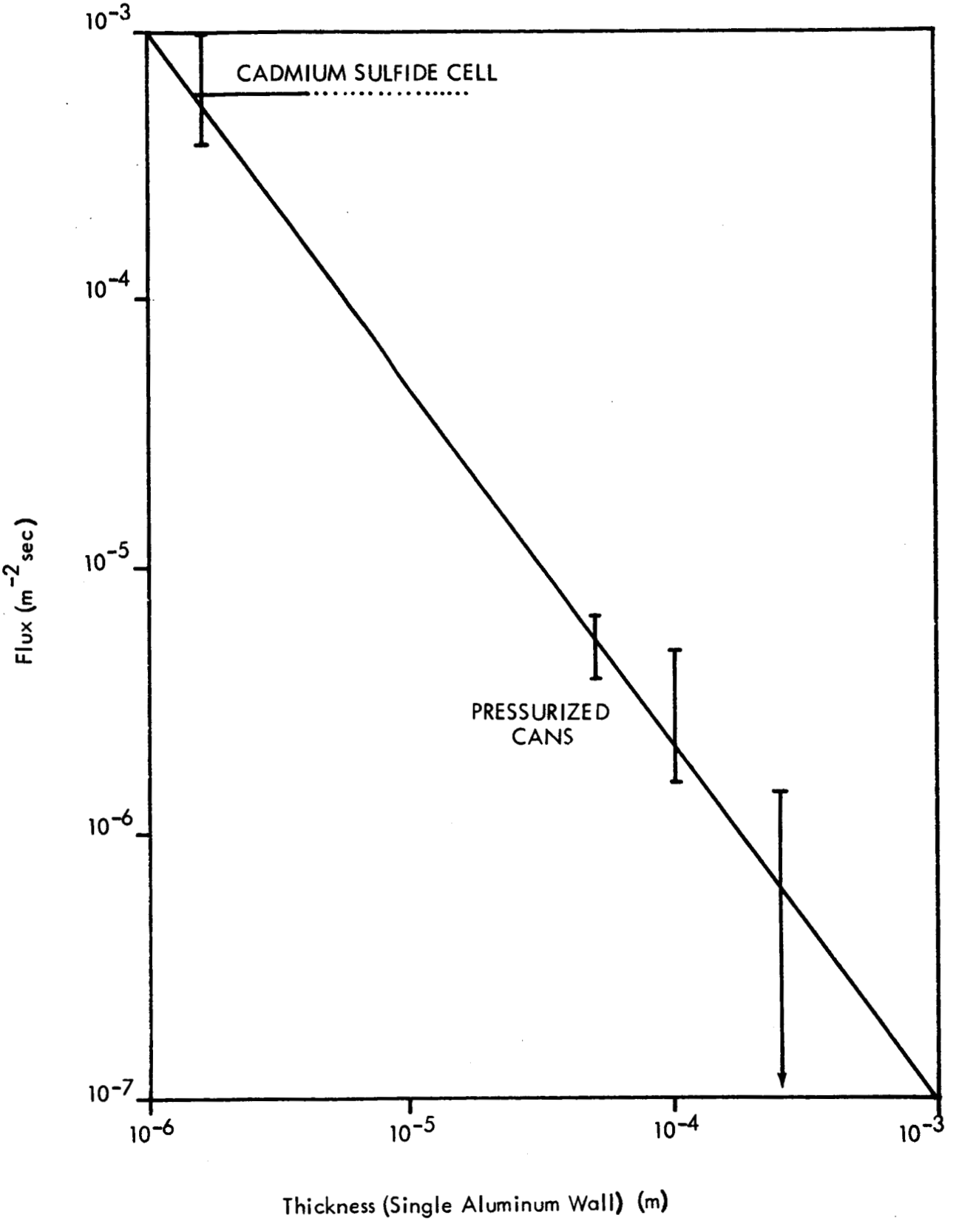

FIGURE 1 CUMULATIVE PENETRATION FLUX MEASURED BY EXPLORER XVI

A final report is in preparation (Secretan, 1964). An interpretation of the flux measurement is shown on Figure 1. The thickness of aluminum equivalent was determined by estimated $(\rho c)^{2/3}$ scaling as 1/3.7 that of mylar. As discussed in Appendix 4, Mr. Secretan will probably treat his data quite differently.

4.3 Summary of Results

The line on Figure 1 is Hastings (63) least squares fit to the pressurized can data. It is interesting that this line passes through the cadmium sulfide cell point. The analytic form of this line is

$$N(T) = N_o T^{-s}. \qquad (4.1)$$

The actual curve (flux, per square meter second, wall thickness of equivalent aluminum, in meters) is

$$\text{Log } N(T) = -11.01 - 1.35 \log T \qquad (4.2)$$

Observing the error limits on the points, this representation is probably an adequate description of the penetrating flux within a factor of two or so over the flux range from 10^{-5} to 3×10^{-7} $m^{-2}sec^{-1}$. For "model" purposes, we extend it upwards to 10^{-3} $m^{-2}sec^{-1}$. We consider that the cadmium sulfide cell result gives some support to this. The points suggest that the flux curve is concave downwards, and we consider equation (4.2) an upper bound on the flux at and below 10^{-7} $m^{-2}sec^{-1}$. In Section 7 of this document, it will be combined with the indirect data to give an over-all hazard model.

4.4 Significance of the Explorer XVI Results

Compared with most hazard models utilized in the past, the hazard of the model based on Explorer XVI data is low. With reference to the first edition of this document, for instance, the penetrating flux at the level corresponding to one mil beryllium copper (5×10^{-5} meters of aluminum equivalent) has been lowered about 30 times. Because the representation of the flux has a small slope, the Explorer XVI line would indicate a flux about five times above that of the old model at a thickness pertinent to Apollo -- say 10^{-3} meters.

A few previous models predict flux levels consistent with the Explorer XVI data. They do not represent the small slope, however, and the agreement must be considered fortuitous.

5.0 THE FLUX OF VISIBLE AND RADIO METEORS

Particulate matter in space is counted by a variety of methods appropriate to the abundance of the bodies. As the flux goes down, the exposure of the experiment must become very large. Thus Brown's collection of meteorites (1960) had an "exposure" of nearly a million square kilometers for a hundred years ($E = 1.6\ 10^{21}$ meters^2 seconds), while some microphone-type detectors used on sounding rockets have exposures as small as 5 m^2 sec and still obtain a reasonable number of counts. For the particles "significant" to Apollo (10^{-9} - 10^{-11} m^{-2} sec^{-1}) and even more, for those significant for prolonged planetary missions, direct measurements of penetration are increasingly difficult. We are forced to depend heavily on ground based studies of the visual and radar meteors.

5.1 Visible Meteors

The most quantitative measurements of the flux of visible meteors were made by Hawkins and Upton (1958) using two Super-Schmidt cameras of the Harvard Meteor Project. Stereoscopic viewing, interrupting shutters, and careful calibration against slewed star fields at the same elevation yield information on position, velocity, acceleration, and the quantitative rate of light generation with time. The data is reduced to the mean photographic magnitude of a meteor traveling parallel to the plate at the zenith.

The "magnitude" of a source is defined in terms of the illuminance, or light flux per unit area, at the observers' position. Generally,

$$M = -2.5 \log_{10} (e/e_o) \qquad (5.1)$$

where M is the magnitude, e is the illuminance, and e_o is the illuminance of a zero magnitude star. For the "visual astronomical magnitude" scale, the Handbook of Geophysics (1961) gives a value of 1.944×10^{-7} ft. candles or 2.094×10^{-6} meter candles for e_o.

The instantaneous magnitude of a meteor is a logarithmic measure of the total luminous flux emitted. The luminous or photographically active flux is assumed a well defined fraction of the energy loss of the meteoroid, so we have

$$I = \tau \frac{d}{dt}\left(\frac{1}{2} m v^2\right) = \frac{1}{2} \tau v^2 \frac{dm}{dt} + \tau m v \dot{v} \qquad (5.2)$$

where I is the luminous flux, m and v are the mass and velocity of the meteoroid, and τ is a "luminous efficiency". The second term in (5.2) can generally be neglected.

One can then compute (from measured values of I) a "photometric mass",

$$m = \int \frac{I}{\tau v^2} \, dt \qquad (5.3)$$

The luminous efficiency is thought to be a linear function of velocity, τ_o v; one obtains

$$m = \frac{1}{\tau_o} \int \frac{I}{v^3} \, dt \qquad (5.4)$$

This formula is the basis for deriving meteor masses. Essentially identical results are accepted by all authorities (Opik 58, Levin 56). The value of τ or τ_o is disputed.

The Hawkins and Upton (58) article gives a distribution of photometric masses. The value of τ_o has shifted around considerably. In 1952, the mass of the zero visual magnitude meteor of 30 km/second velocity was .15 grams; in 1958, 30 grams; Whipple (63) now uses 1 gram, and Hawkins prefers 4.4 gm. With the one gram normalization, the observed flux mass relation is

$$\log N = -18.20 - 1.34 \log m \quad (m^{-2} \text{ sec}^{-1}, \text{ kg}) \qquad (5.5)$$

The empirical range of this formula is approximately

10^{-3} kg $> m >$ 10^{-5} kg.

Whipple (63) includes a term explicitly involving meteoroid density. As stated in the introduction (and in Hawkins and Southworth 63), the measured, deceleration-density is applicable only to characterization of individual dust ball fragments. It must not be included.

Equation (5.5) has been chosen as an Apollo model, and is fixed by the document, Natural Environment and Physical Standards for Apollo (1963). It should be emphasized that, as described in Appendix 5, there are considerable uncertainties in the value of τ_o. In particular, the chosen value depends strongly on an assumed chemical composition of the cometary meteoroids, about which almost nothing is known.

5.2 Radio Meteors

Three NASA research reports have been published from the data of the Harvard Radio Meteor Project (Hawkins 63, Hawkins and Southworth 63, Hawkins, Lindblad, and Southworth 63).

The average velocity of radio meteors decreases from about 38 km/second at about the sixth magnitude to 36.2 km/second at magnitude 8.6 and perhaps 32 km/second at about magnitude 9. The meteors appear more fragile than visible meteors, and the flux (at 4×10^{-4} grams) is reported perhaps an order of magnitude above the relation (5.5). The Hawkins and Southworth report contains a tabulation of 327 meteors, "all for which heights could be obtained during the period from November 1961 to March 1962." This is otherwise a random sampling, containing only a few stream meteors. Masses are computed from electron density in the trail by a technique analogous to that employed in (5.3) for visual meteors. Again, estimated values depend strongly on meteoroid composition.

The investigators have not published their mass-flux results as yet. However, looking at the tabulated data, the most massive particles are about 4.4×10^{-2} grams, or 5th magnitude on Hawkins scale (0 magnitude meteor, 4.4 grams). A cumulative distribution of numbers is shown in Figure 2. It has a clear slope of -2, and is well defined for a factor of 10 in mass (to magnitude 7.5). Above this the data drops away in a manner which could be instrumental. The limiting mass is about 4×10^{-4} grams (magnitude + 10).

5.3 Flux Mass Relation

The Whipple (63) flux mass relationship, equation (5.5), is plotted on Figure 3. The square law radio meteor flux is joined at the 5th magnitude (10^{-5} kg). The analytic form for this is

$$\log N = 21.5 - 2 \log m \quad (m^{-2}\ sec^{-1},\ kg) \qquad (5.6)$$

m is approximately $10^{-5} > m > 10^{-6}$ kg.

The uncertainties in these fluxes are mainly in mass, where they arise principally from arbitrary assumptions about meteoroid composition. We concur with Hawkins on an uncertainty of $10^{\pm 0.7}$.

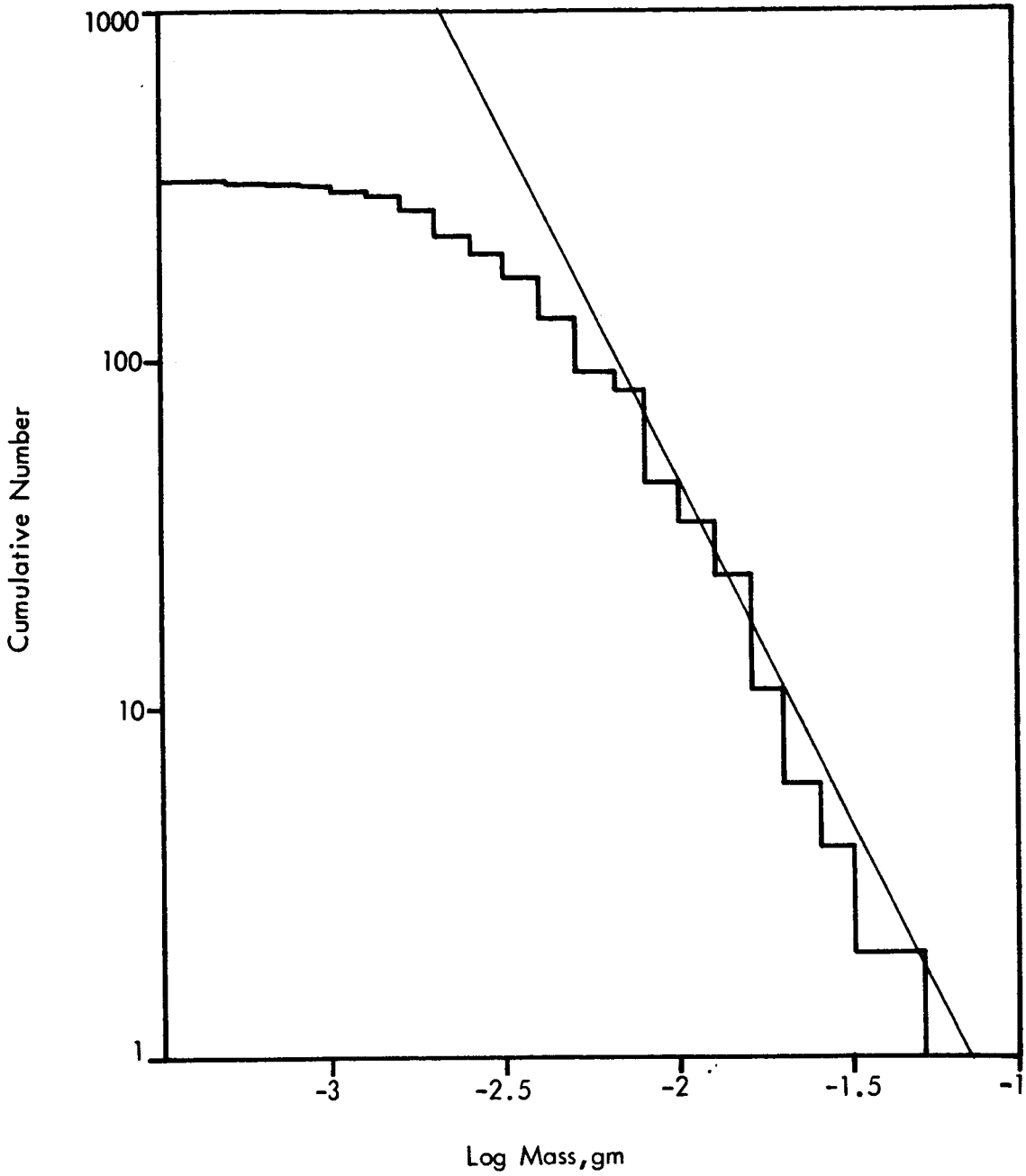

FIGURE 2 CUMULATIVE NUMBER-MASS DISTRIBUTION FOR RADAR METEORS.

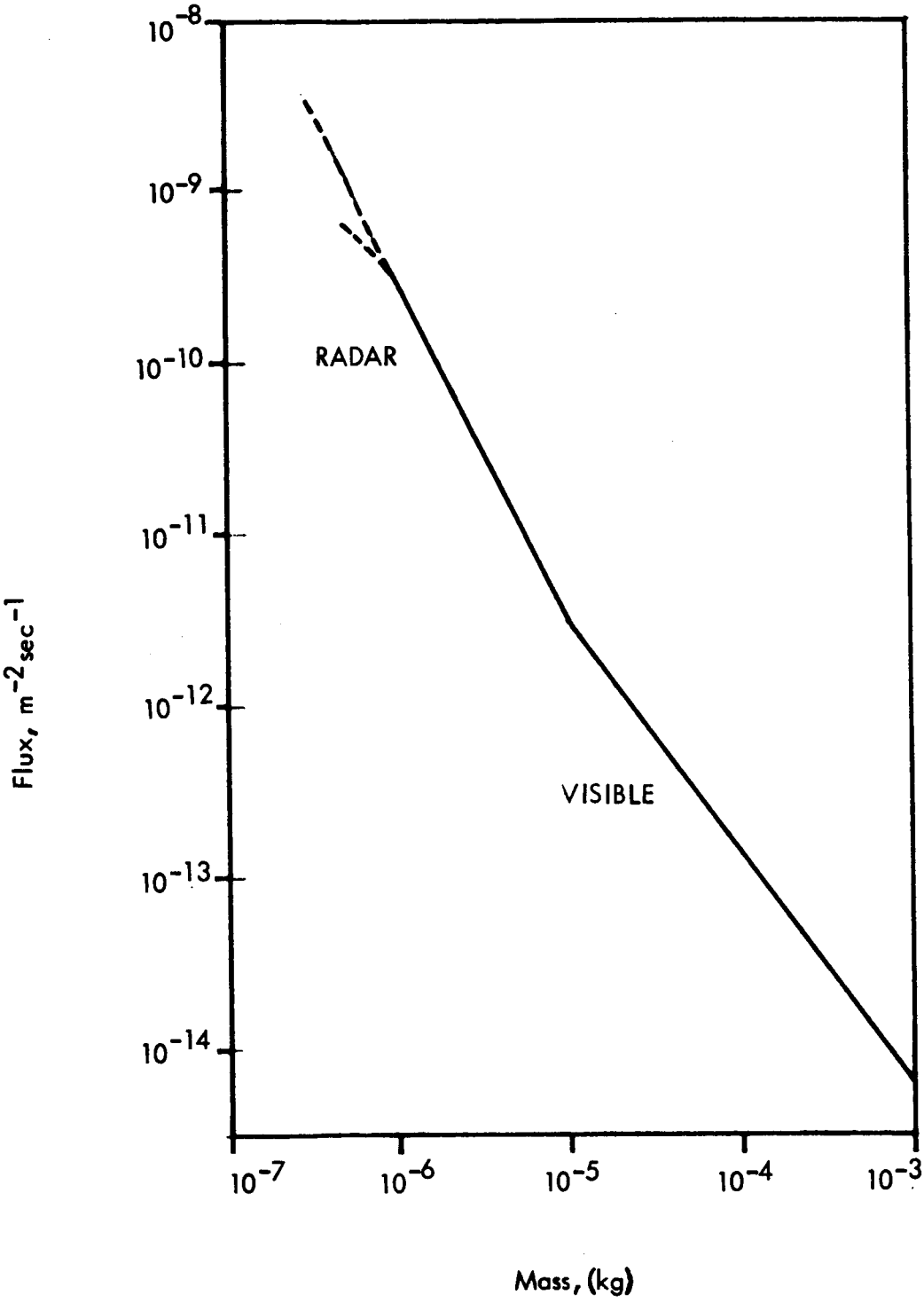

FIGURE 3 CUMULATIVE MASS-FLUX OF VISIBLE AND RADAR METEORS (Zero Magnitude Mass, 1gm)

6.0 PENETRATION ENVIRONMENT (METEOR DATA)

In the above sections, we have defined a penetration flux for Explorer XVI, chosen a penetration criterion, and written expressions for the flux of visible and radio meteors. The latter may be combined to derive an indirect penetration flux, and the results compared with the direct data.

Since we wish to compute puncture probability, in a standard aluminum skin, we use equation (3.9).

$$T = 0.41 \left(\frac{\rho_p}{10^3}\right)^{1/3} \left(\frac{v \cos \theta}{10^4}\right)^{1/2} \qquad (6.1)$$

The model for visual meteors (Natural Environment, 63) specifies a meteoroid density of 0.5 gm/cc, or 500 kg/m^3. It appears that this value may be incorrect, or at least chosen for the wrong reason. It is clear that the "densities" given by the radar measurements are no more than convenient estimates of the number of fragments. B. J. Levin (56) has questioned the densities obtained for visual meteors on the same grounds, and prefers 2 gm/cc for a nominal value, characteristic of the packing of the meteoroid in space. To emphasize the uncertainty, we assign the density a nominal value of one, with an uncertainty of three times. The density becomes $\rho_p = 10^{\pm 0.5}$ gm/cc.

Other parameters for the penetration law are summarized in Table 6.1. An estimated error of 5x is assigned (after Hawkins) to meteoroid mass. The average velocity of the radio meteors is 38 km/sec; that of the visual meteors, 30 km/sec.

The uncertainties in density and in mass are propagated as though independent errors -- that is, the logarithmic error in a product is the square root of the sum of the squares of the logarithmic errors of the factors.

TABLE 6.1

Penetration Hazard Model: Indirect Measurements.

Wall just punctured = 1.8 p

Particle density $10^{3\pm0.5}$ kg/m^3

Target density 2.7×10^3 kg/m^3; sound velocity, 5.1 km/sec (Aluminum)

Aspect ratio: unity

Uncertainty in meteoroid mass. 5 times

Average normal velocity: one half meteoroid velocity

Units in Table: all fluxes, m^{-2} sec^{-1}; all masses, kg; all thicknesses, m.

Visual Meteor Model

$$\log N = - 18.20 - 1.34 \log m \pm 0.94 \qquad (6.2)$$

$$\log T = - 0.30 + (1/3) \log m \pm 0.17 \qquad (6.3)$$

$$\log N = - 19.41 - 4.02 \log T \pm 1.16 \qquad (6.4)$$

Range of validity: log N, - 11.50 - 14.20
log T, - 1.97 - 1.30

Radio Meteor Model

$$\log N = - 21.50 - 2 \log m \pm 1.40 \qquad (6.5)$$

$$\log T = - .25 + (1/3) \log m \pm 0.17 \qquad (6.6)$$

$$\log N = - 22.98 - 6 \log T \pm 1.73 \qquad (6.7)$$

Range of validity: log N, - 9.50 - 11.50
log T, - 2.24 - 1.91

Other Models

Whipple (63)

$$\log N = - 21.37 - 4.02 \log T \qquad (6.8)$$

Orrok (63)

$$\log N = - 16.70 - 3 \log T \pm 1.16 \qquad (6.9)$$

The nominal lines with the error band are plotted on Figure 4, together with the Whipple (63) model and the error envelope of the Orrok (63) model from the first edition of this document.

The hazard from the visual meteors appears radically different for the present paper and for the Whipple model, from which the mass flux was taken. Firstly, Whipple's equation represents a "near earth" flux, and therefore is smaller by two times. Beyond this, he chooses the Hermann and Jones (HIS 62) logarithmic penetration criterion (which depends strongly on material strength and on projectile density (Appendix 3)) and different values for several parameters -- in particular, a meteoroid density of 0.44 gm/cc and a mean velocity of 22 km/sec. We are in disagreement by 2.65 times in penetration, or $(2.65)^{4.02} = 50$ times in flux. This is discussed Appendix 6.

With regard to the hazard relation presented in the first edition of this document, the old and new error envelopes are essentially coincident in the significant range for Apollo. The author would like to take credit for this, but fears it is fortuitous.

For very long exposure missions, the estimate of hazard is substantially reduced, since the steep slope of the present visible meteor flux deemphasizes larger particles.

In the next section, we join the direct and indirect estimates of penetrating flux. It will be seen that they can be joined smoothly together.

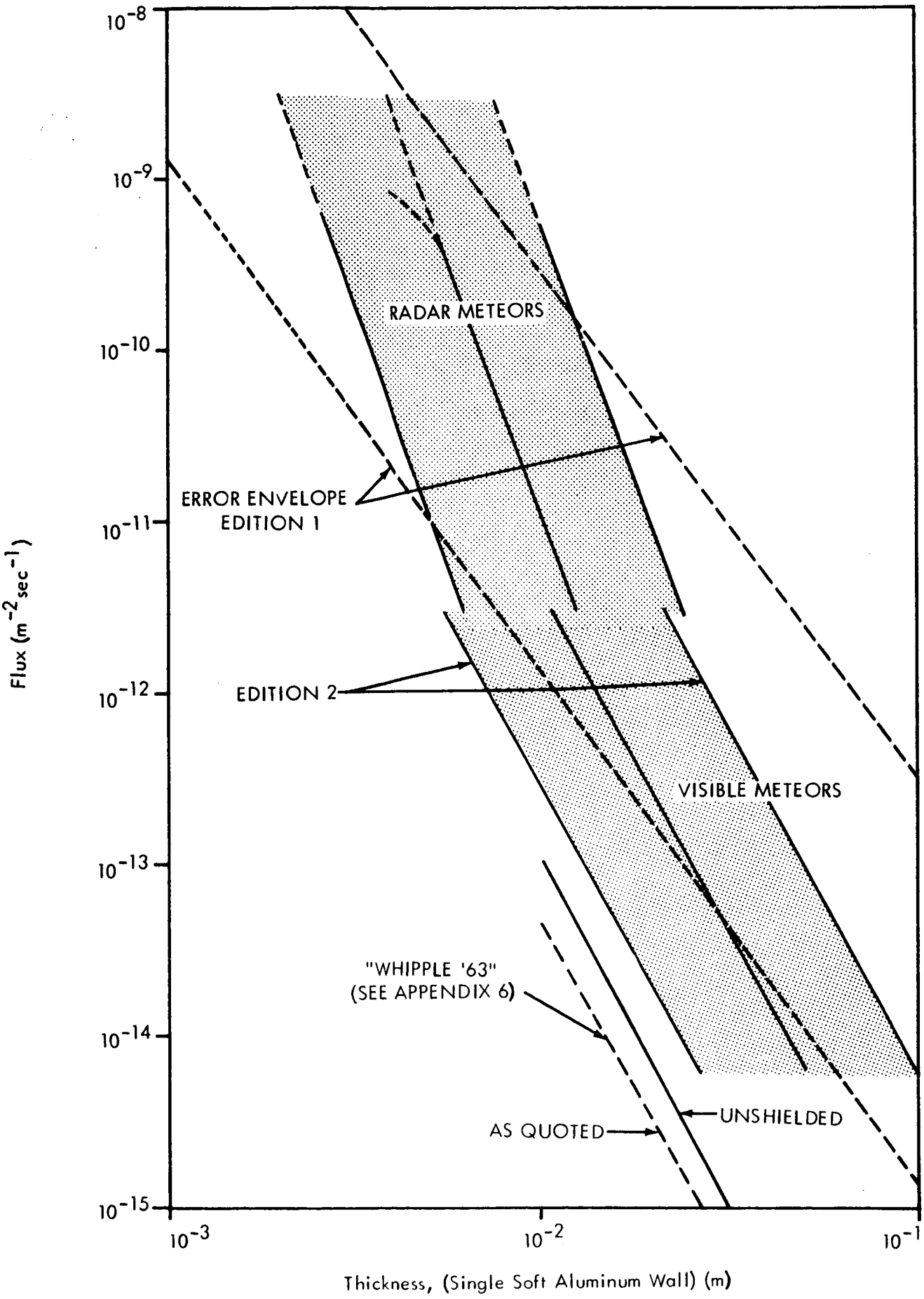

FIGURE 4: CUMULATIVE PENETRATION FLUX, VISIBLE AND RADAR METEORS

7.0 OTHER FLUX DATA: UNIFIED PENETRATING FLUX MODEL

We have established above estimates of the meteoroid puncture environment based on the Explorer XVI direct measurements, and on the indirect observation of visual and radio meteors. There exists a considerable body of information obtained by other earth satellites over the years -- both penetration and microphone impact measurements have been made. Explorer XVI exhibits far lower puncture rates than the first and is in clear contradiction with the second. Presumably this contradiction reflects our ignorance about the nature of dustballs. The data are shown in Figure 5.

7.1 Other Direct Measurements

At least seven satellites have carried experiments designed to measure the flux of particles penetrating some target. In Appendix 4, the penetration criterion has been used to convert the actual thicknesses to "equivalent aluminum". This may be particularly questionable for the wire-grid targets, which require the severing of a wire for an indication. Most of these experiments have very small exposures and show no punctures. These have not been plotted.

The few points representing actual damage are generally well above the Explorer XVI data. These are shown on Figure 5. It should be noted that the exposures of all these experiments are 10^{-3} that of Explorer XVI or less, with the single exception of Vanguard III; no punctures were detected, and the "empty" point is shown on Figure 6. It corroborates the 5 mil beryllium copper point.

It is reasonable to exclude the others, even were the exposures comparable. Briefly, the two at $3.2\ 10^{-5}$ meters are wire grid experiments. Severing a wire is not simply comparable with a plate penetration experiment. A particle which would just not penetrate a plate of thickness T could completely destroy a wire of diameter T. Yet for lack of better information, plate thickness and wire diameter have been assumed equivalent in plotting Figure 5. The points should be moved to the left an unknown amount.

Of the other two data points, at 1.6×10^{-6} meters, the Explorer VII result is a cadmium sulfide cell experiment similar to that flown on the Explorer XVI, but with 100 times smaller exposure. It sustained only one puncture. The last is, to date, the only recovered meteoroid target, the Venus Flytrap recoverable sounding rocket (Hemenway and Soberman, 63). Collection boxes were opened at an altitude above 100 km. These collected a very large number of particles, and three penetrations were found in

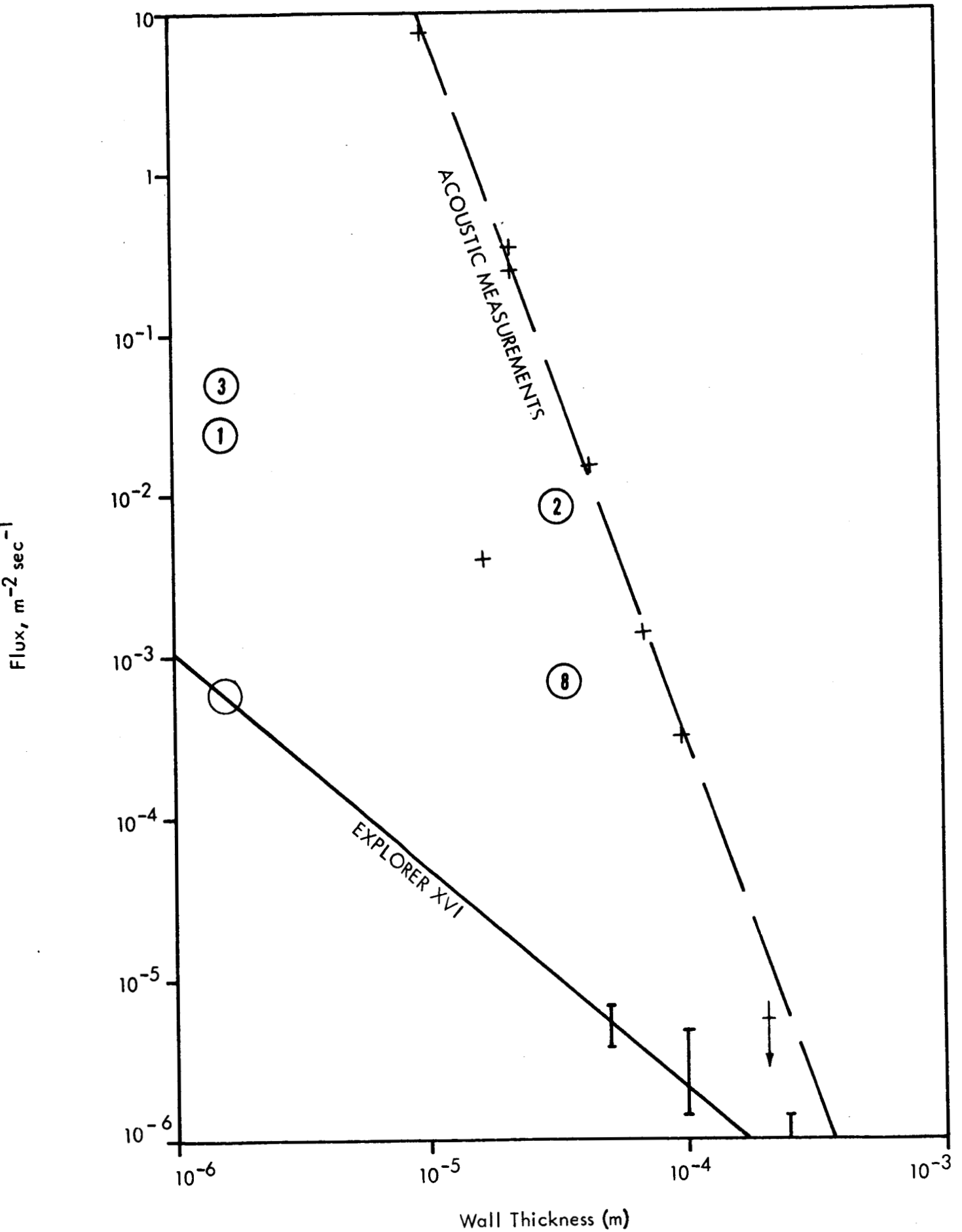

FIGURE 5 CUMULATIVE PENETRATION FLUX: +, ACOUSTIC MEASUREMENTS; (N), PENETRATION MEASUREMENT, "N" EVENTS.

six micron mylar film. The particles were apparently falling at terminal velocity. The penetrations are not hypersonic, the holes being much larger than the target thickness.

To conclude, it seems reasonable to exclude these data in constructing a penetration flux curve.

7.2 Other Indirect Data: Acoustic Measurements

Many satellites have carried microphones sensitive to the momentum of incident particles; thousands of impacts have been recorded. Calibration is conventionally performed with low velocity particles, but has been checked with projectiles accelerated to five or six kilometers per second (Kells and Keough 58). The calibration constants are currently under review at Goddard Space Flight Center. Possible corrections amounting to as much as a factor of three may appear.

The acoustic measurements exhibit good statistics and are self-consistent over a large range of fluxes. To plot these, equation (6.1) is rewritten:

$$T = 0.41 \left(\frac{\rho_p}{10^3}\right)^{1/3} \left(\frac{v \cos \theta}{10^4}\right)^{1/6} \left(\frac{P \cos \theta}{10^4}\right)^{1/3} \qquad (7.1)$$

where P is the particle momentum.

It is customary to assume a somewhat lower velocity than for the meteors. We choose $1.8\ 10^4$ meters per second. Further treatment of the data is covered in Appendix 4, and the result is plotted on Figure 5. It will be noted that the acoustic fluxes are far above the Explorer XVI data. They are not inconsistent with an extrapolation from the photographic meteor results.

Deep space probes (Pioneer and Mariner) show much smaller fluxes than this.

Alexander et al (62) have shown that the older penetration observations are less discordant with the microphone measurements if penetrating particles are characterized by diameters approaching the "critical dimension for fracture" (i.e., plate thickness for example) of the detector, rather than by a penetration law (equation 7.1). This again emphasizes our lack of understanding of the nature of the projectiles.

7.3 Penetrating Flux: Best Estimate

In the high flux region, Explorer XVI represents data directly applicable to hazard estimates. In the lower

fluxes, we have no choice but to use the visible and radio meteors. In Tables 7.1 and 7.2, the analytical forms and the assumptions used are tabulated. In Figure 6, error envelopes have been plotted, and smoothly joined. In extrapolating the pressurized can results, each envelope line passes through two 90% confidence limit points. The 5 mil beryllium copper can and the Vanguard III experiments are represented as arrows with fleches at the flux for 10% probability of no puncture (upper) and 50% probability of no puncture (middle). The error envelope is biased slightly downwards in accord with the data.

Clearly, these data are not inconsistent, and within their errors may be combined as a single set. On Figure 7, the nominal lines and error envelopes have been plotted, and the termination of the radio meteor data connected by a straight line with the chosen extrapolation limit of the Explorer data. The equation of this line, labeled "Interpolation", is included in Table 7.2. Figure 7, with the tables, represents our current "best estimate" of puncture hazard over the entire flux range.

Comparing this model with that of Edition 1, considerable "structure" has been introduced in the flux-penetration relation. It will be noted (Figure 6) that the estimated error in penetration has been slightly reduced, in the significant range for spacecraft. This change, from 2.5x to about 2x, is a result of the radio meteor data, which tie these fluxes definitely to the zero visual magnitude meteor. Edition 1 included an estimated error in extrapolation of the visual meteor data, which has been eliminated. If our interpretation of the radar data is in error, the earlier uncertainty will return.

It should be emphasized that because the radar flux curve is "steep", the uncertainty in <u>flux</u> exceeds that in Edition 1.

With regard to the magnitude of the new estimate, the change from the old model is under three times from fluxes of 10^{-6} to 10^{-11} m^{-2} sec^{-1}, covering the significant ranges for both astronauts and spacecraft. This change is barely meaningful within the error estimates. The small amount of the change is explained in part by the fortuitous cancellation of various alterations in the model, and in part by the lack of important changes in our understanding of the physical situation.

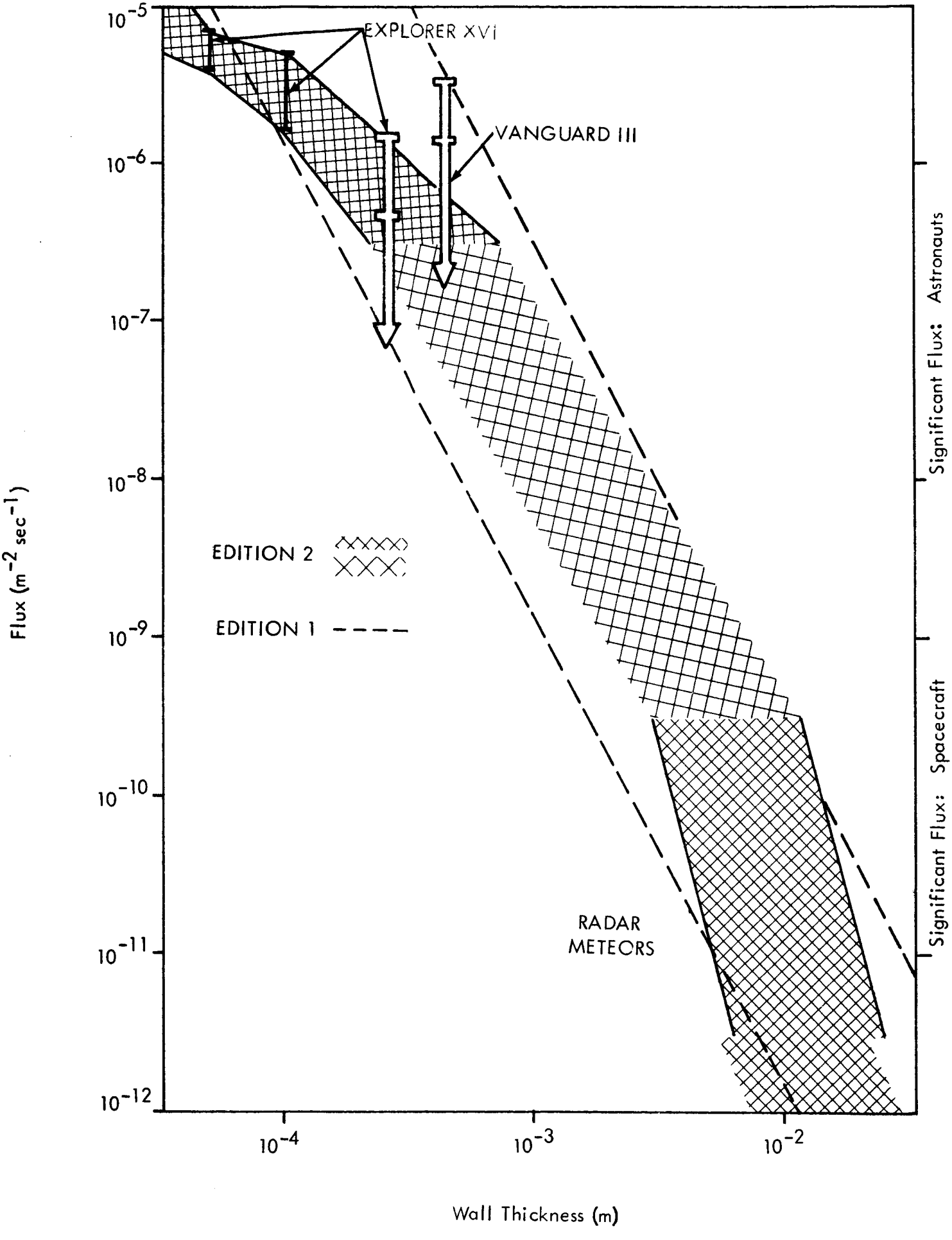

FIGURE 6 ESTIMATED ERROR ENVELOPE: PENETRATING FLUX

TABLE 7.1

CONSTRUCTION OF PENETRATION FLUX MODELS

Explorer XVI: Hastings (63) least squares fit to pressurized can data.

Visual Meteors: Hawkins and Upton (58) flux-photometric mass equation. The mass scale is reduced 30x to obtain a one gram mass for the zero visual magnitude (-1.8 photographic magnitude) meteor.

Radio Meteors: Hawkins and Southworth (63) flux-radio mass data. The mass scale is reduced 4.4x to obtain a one gram mass for the zero visual magnitude meteor at 30 km/sec.

Meteoroid Mass Uncertainty: $10^{\pm 0.7}$ (caution: this fails to bracket Hawkins' radio estimate).

Meteoroid Density: $10^{\pm 0.5}$ gm/cc.

Penetration Law: Ames criterion (Summers 59) modified to a $v^{1/2}$ dependence above 10 km/second, and including a dependence on the normal component of projectile velocity.

TABLE 7.2 PENETRATION FLUX MODEL

Source	Flux Range $\log_{10}, m^{-2} sec^{-1}$	Thickness Range $\log_{10}, m$	logarithmic equation	Estimated log error, flux
Explorer XVI	-3, -6.5	-6, -3.36	log N = -11.01 - 1.35 log T	±0.3*
Interpolation	-6.5, -9.5	-3.36, -2.24	log N = -15.5 - 2.68 log T	
Radar Meteors	-9.5, -11.5	-2.24, -1.91	log N = -22.98 - 6 log T	±1.73**
Visual Meteors	-11.5, -14.2	-1.97, -1.30	log N = -19.41 - 4.02 log T	±1.16**

Thicknesses penetrated in other materials shall be estimated by $(\rho c)^{2/3}$ scaling (equation 3.7) or, preferably, by reference to controlled experimental data.

* only in the range $-5 > \log T > -6.5$

** error in thickness, ±0.29

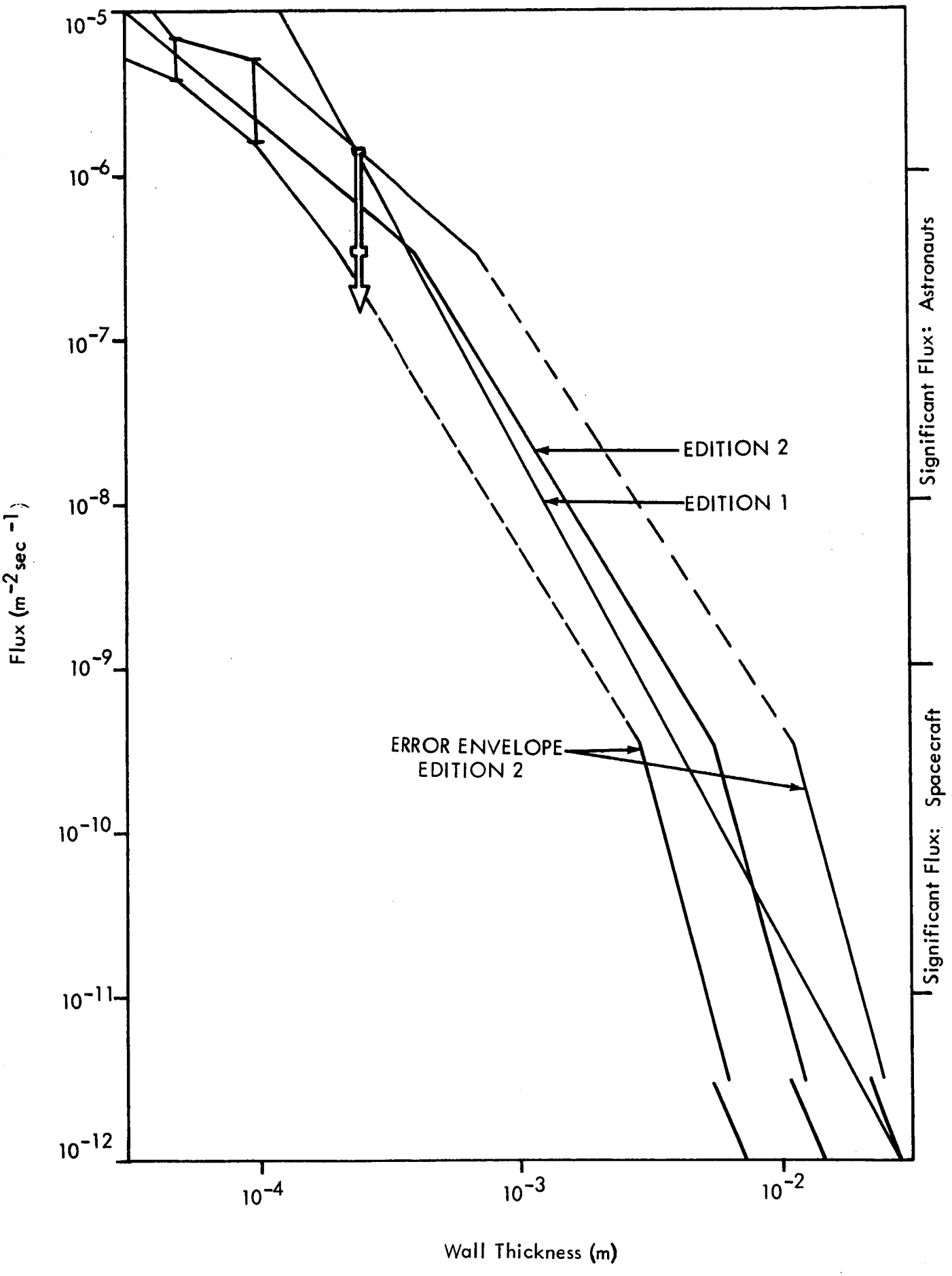

FIGURE 7 PENETRATING FLUX

8.0 SPACE DEPENDENCE OF THE METEOROID HAZARD

8.1 Concentration Near the Earth

Principally on the basis of the acoustic measurements, it has been hypothesized that there is a dust cloud around the earth. The hazard presumably would decrease as one moved into cislunar space.

There is no evidence for such a cloud in the significant range for puncture of the Apollo spacecraft. The data from the visual and radio meteors is obtained with excellent velocity information. It is evident that these particles are in solar orbit and cannot be concentrated near the earth.

It should further be noted that the theoreticians (or at least half of them) have difficulty imagining how substantial particles could get into such orbits.

8.2 Concentration Near the Moon

Gault, Shoemaker, and Moore (63) have discussed the problem of the density of fragments ejected from meteoroid impacts on the lunar surface. They estimate that the flux is very much increased, although the particles have low velocity. Boyle and Orrok (63) have calculated the expected increase in penetration rate, assuming that penetration is proportional to the kinetic energy of particles. Since kinetic energy is at the most conserved in a primary impact, the secondaries cannot double the energy influx. Under reasonable assumptions about the kinetic energy distribution among secondary fragments, the penetration rate cannot be doubled.

8.3 Conclusions

There do not appear to be strong arguments supporting increased hazard estimates near the earth or near the moon. Particularly in the case of the fluxes significant for Apollo spacecraft penetration, where the uncertainty in the estimate in low earth orbit is already more than an order of magnitude, it seems possible to ignore space dependence of hazard.

9.0 EROSION HAZARD

Meteoritic erosion implies the gradual coverage of a spacecraft with small pits. The "coverage time" in which a given area is entirely covered with pits is the reciprocal of an "erosion rate". For times much shorter than the coverage time, the attack will be irregular.

The model for the flux of penetrating meteoroids enables the approximate calculation of coverage times.

9.1 Erosion Rates from Penetrating Flux

It is easy to calculate the crater area opened up per unit area and unit time by a meteoroid influx (see Orrok, 64). The nature of the result depends upon the flux distribution. Considering the distributions in penetration (which will be similar to the distributions in particle size and crater diameter), if the exponent is high, as in the visual meteor flux, the small particles dominate, and coverage is controlled by the very highest fluxes. On the other hand, if the exponent is below 2 (the Explorer result is, of course, 1.3), the largest particles dominate -- i.e., open out more area per unit time than the small. In this case, the erosion hazard is operationally indistinguishable from the puncture hazard, and need not be further considered for Apollo. The result is not inconsistent with other data.

The dominant particle for the measured penetrating flux is (referring to Figure 6) the particle with a flux of 10^{-7} m^{-2} sec^{-1}, which penetrates 10^{-3} meters of aluminum. To an order of magnitude, the rate of coverage, C, is just the cumulative flux times crater area.

$$C = NT^2 \tag{9.1}$$

We approximate the crater diameter by the penetration T and ignore constants near one (see the referred article).

For the stated values, we obtain

$$C \sim 10^{-13} \frac{m^2}{m^2 \text{ sec}} . \tag{9.2}$$

That is, 10^{-13} of the area of the surface is opened up by meteoroid cratering each second. One hundred percent coverage (not allowing for overlap) would be attained in a few hundred thousand years. The equivalent erosion rate would only be defined over times of this order but is, since the "coverage" extends 10^{-3} meters deep,

$$\frac{10^{-3} \text{ meters}}{10^{5.5} \text{ years}} \sim 30 \text{ Angstrom units per year.}$$

This value is consistent with other estimates. F. Whipple (63a), for instance, suggests from studies of the radio "ages" of meteorites that an erosion rate of 12 AU/yr makes good sense.

McKeown and Fox (62) report a measurement of the erosion of a gold surface in low earth orbit (Discoverer 26). The erosion is .2 ± .1 AU/day, or 70 Angstrom units/year. This is attributed entirely to sputtering.

9.2 Conclusion

Our conclusion is that the deep space erosion hazard is due to larger particles and is operationally indistinguishable from a puncture hazard. The near-earth environment probably offers a modest erosion rate due to sputtering.

The distribution of secondary ejecta near the lunar surface may contain more penetrating small particles than the primary flux -- that is, although puncture hazard is unaffected, the erosion hazard will be different. Happily, estimates of erosion rate are startlingly indifferent to the fluxes employed. Use of the "model" of the first edition yields a rate approximating thirty Angstrom units a year, with a coverage time of perhaps six thousand years. The secondary distribution at the lunar surface is very unlikely to exceed this value.

10.0 CONCLUSIONS

An attempt has been made to define the hazards to Project Apollo associated with particulate matter in space. Where information is clearly available to us, it has been used. Where information has been lacking, reasonable assumptions have been made.

Such a "model" has general usefulness only insofar as it is up to date, and as its deviations from other proposed models are either justified or explicitly allowed by error estimates.

Since the first edition, the situation has become better defined. The description of the environment necessarily becomes more complicated as valid information accumulates, and before scientific insight is available to simplify the relationships involved.

It is felt that the estimate of penetration hazard is "good", although, as exemplified by Professor Whipple, it is possible for serious workers to disagree strongly.

Improvements in the estimate should arise from the SA-9 and SA-8 shots (Appendix 7) and from the "simulated meteor experiments" which should unambiguously tie together the visual and radio meteor data.

Uncertainties in the indirect data will remain, since the composition and structure of dustballs will still be unknown. The usefulness of direct data will be limited unless unambiguous proof tests of meteoroid bumpers can be made, either in space or in the laboratory.

The estimate of erosion hazard is considered satisfactory. Large errors in the flux would still not produce significant erosion.

G. Timothy Orrok

G. T. Orrok

GTO/tj

Acknowledgements

I am indebted to a number of people for information contained in this document. In particular, I should like to thank the members of the Meteoroid Technology Advisory Working Group and the chairman, C. D'Aiutolo, through whom I received early returns on the Explorer XVI data. I am grateful to L. Secretan for my glance at the Cadmium Sulfide Cell data. B. T. Howard and W. S. Boyle made helpful suggestions on the text. The efforts of the Misses G. Jefferson, S. Peery, and M. Feild were invaluable.

REFERENCES

Alexander, W. M., C. W.McCracken, L. Secretan and O. E. Berg, COSPAR, (May 1962).

Bjork, R. L., Rand Corporation Report, P1662, (1958).

Boyle, W. S. and G. T. Orrok, AIAA Jour., 1, 10, pp. 2402-2404.

Brown, H., J. Geophys. Research, 65, 6, pp. 1679-1683, (1960). See also addendum to this article: J. Geophys. Research, 66, 4, pp. 1316-1317, (1961).

Charters, A. C., and G. S. Locke, Jr., NACA Report A58B26, (1958).

Cook, Allan F., L. G. Jacchia and R. E. McCrosky, Smithsonian Contributions to Astrophysics, 7, pp. 209-220, (1963).

Gault, D. E., E. M. Shoemaker and H. J. Moore, NASA Technical Note, TND - 1767, (April 1963).

Handbook of Geophysics, rev. ed., USAF, Macmillan, New York, (1961).

Hastings, E. C., Jr., NASA TMX 810, (February 1963), NASA TMX 824, (April 1963), NASA TMX 899, (September 1963).

Hawkins, G. S., B. A. Lindblad and R. B. Southworth, Radio Meteor Project, Research Report Number 1, (June 1963), NASA Contract NASr-158.

Hawkins, G. S. and R. B. Southworth, Radio Meteor Project, Research Report Number 2, NASA Contract NASr-158, (July 1963).

Hawkins, G. S. and E. K. L. Upton, Astrophys. J., 128, 3, pp. 727-735, (1958).

HIS, Proc. of Fifth Hypervelocity Impact Symposium, Tri Service Committee, Contract Number Nonr (G) - 0020-62 (X), (1962).

HIS, Proc. of Sixth Hypervelocity Impact Symposium, Tri Service Committee, Contract Number DA-31-124-ARO(D)-16, (1963).

Kells, M. C. and D. D. Keough, Astia Document AD 21093, (1958).

Levin, B. J., The Physical Theory of Meteors (Ch. I-III), translated, Am. Met. Soc., Astia AD 110091, (1956).

McCrosky, R. E. and R. K. Soberman, Smithsonian Contributions to Astrophysics, 7, pp. 199-208, (1963).

McKeown, D. and M. G. Fox, ARS Journal, pp. 954-955, (June 1962).

McKinley, D. W. R., Meteor Science and Engineering, McGraw-Hill, New York, (1961).

Natural Environment and Physical Standards for Apollo, OMSF Program Directive, M-DE 8020.008A, (August 15, 1963). (conf)

Opik, E. J., Physics of Meteor Flight in the Atmosphere, Interscience, New York, (1958).

Opik, E. J., Irish Astronomical J., 5, pp. 14-23, (1958a).

Orrok, G. T., Meteoroid Environment of Project Apollo (Ed. 1), Bellcomm Technical Report, (January 31, 1963).

Orrok, G. T., Meteoric Infall and Lunar Surface Roughness, Bellcomm Technical Report, (January 31, 1964).

Soberman, R. K., C. L. Hemenway, T. G. Ryan, S. A. Chrest, J. Frissora and E. F. Fullam, Smithsonian Contributions to Astrophysics, 7, pp. 89-92, (1963).

Summers, J. L., NASA TND-94, (October 1959).

Watson, F. G., Between the Planets (Revised), Harvard University Press, Cambridge, Massachusetts, (1956).

Whipple, F. L., J. Geophys. Research, 68, pp. 4929-4939, (1963).

Whipple, F. L., Smithsonian Contributions to Astrophysics, 7, pp. 239-247, (1963a).

APPENDIX 1

Table of Symbols used in text:

Certain symbols defined and used only in one appendix are not included in this list.

A — Aspect ratio of projectile: ratio of dimension along line of flight to the geometric mean of dimension transverse to the line of flight (equation 3.4).

B — Bumper factor: the ratio of the thickness of a single wall to the total thickness of a double wall having equal resistance to meteoroid penetration.

C — Coverage: the fraction of surface area covered with craters in some elapsed time (overlapping craters are counted independently).

c, c_1, c_2 — The velocity of sound in a material. Subscripts distinguish particular materials.

D_c — Crater diameter.

d — A particle dimension, measured along the line of flight.

E — "Exposure" or area - time product of a space mission.

e — "Illuminance": the light flux (in lux) incident in a surface near the observer.

e_o — The illuminance of a zero absolute visible magnitude star.

H, H_1, H_2 — The Brinnell Hardness Number of a target. Individual materials may be distinguished by subscripts.

M — The visual magnitude of a light source.

M_{pg} — The photographic magnitude of a light source.

m, m_p — The projectile mass.

$N(x)$ — Cumulative flux m^{-2} sec^{-1} of all particles having values of a property exceeding x (i.e., mass, diameter, thickness just penetrated, etc.).

N_o — A constant in a flux law (equation 4.1).

P_o Probability of zero impacts in a space mission.

P_1 Probability of one impact in a space mission.

p, p_1, p_2 Crater depth resulting from impact. Subscripts distinguish different target materials.

s Exponent in flux law (equation 4.1).

T, T_1 Thickness of a wall. Subscripts may distinguish different materials or structures.

V_t Volume of a crater in a target.

V_p Volume of a projectile.

v Speed of a particle.

$\dot{v}$ Acceleration of a particle.

ρ_p Density of projectile.

ρ_t Density of target.

Φ Total luminous flux from a source.

θ Angle of incidence of projectile (measured from the normal).

τ Luminous efficiency.

APPENDIX 2 THE MAJOR METEOR SHOWERS

Shower	Date of Peak Activity	Radiant Coordinates R.A.	Radiant Coordinates Dec.	Duration of Peak, days	Observed Velocity V_o, km/sec	Fractional Rate Increase
Quadrantids	Jan. 3	231°	+50°	0.5	41	6x
Corona Australids	Mar. 16	245	-48	(5)	--	1.5x
Virginids	Mar. 20	190	00	(20)	30	1.5x
Lyrids	Apr. 21	272	+32	2	48	1.5x
Eta Aquarids	May 4	336	00	10	64	3x
Arietids (D)	June 7	45	+23	20	39	7x
Zeta Perseids (D)	June 9	62	+24	15	29	5x
Ophiuchids	June 20	260	-20	(10)	--	(3x)
Beta Taurids (D)	June 29	87	+20	10	31	3x
Capricornids	July 25	315	-15	(20)	--	3x
Southern Delta Aquarids	July 29	339	-17	15	41	3x
Northern Delta Aquarids	July 29	339	00	20	41	2x
Pisces Australids	July 30	340	-30	(20)	--	3x
Alpha Capricornids	Aug. 1	309	-10	(25)	23	1.5x
Southern Iota Aquarids	Aug. 5	338	-15	(25)	35	2x
Northern Iota Aquarids	Aug. 5	331	-6	(25)	30	2x
Perseids	Aug. 12	46	+58	5	60	6x
Kappa Cygnids	Aug. 20	290	+55	(3)	26	1.5x
Orionids	Oct. 21	95	+15	5	66	3x
Southern Taurids	Nov. 1	52	+14	(45)	29	1.5x
Northern Taurids	Nov. 1	54	+21	(30)	30	1.5x
Leonids	Nov. 16	152	+22	4	72	1.5x
Phoenicids	Dec. 5	15	-55	(0.5)	(13)	6x
Geminids	Dec. 13	113	+32	6	35	6x
Ursids	Dec. 22	217	+80	2	34	2.5x

APPENDIX 3

Penetration Criteria

In this appendix we explain our choice of penetration criterion and indicate its probable accuracy.

Estimates as to crater depths resulting from hypervelocity impact come from two sources, experiment and hydrodynamic theory.

Firstly, there is a vast body of experimental data. Hermann & Jones (HIS 62) have performed a major job of collecting available data released prior to April 1961. The data largely concern the velocity range of 0.5 - 3 km/second. In a few cases data extend to 5 km/second. Individual workers have investigated the higher speed range, to 9 or 10 km/second.

This body of information is in the open literature, and a vast number of "penetration criteria" represent no more than empirical fits to one sub-set or another of this data. Extrapolation of these fits to the meteoritic impact regime is then a matter of judgment. Are the same physical processes active? If so, the data fit is a "representation" of the physical result, like the first few terms of a Taylor expansion. Is the fit sufficiently good that one can have confidence that higher terms are unimportant?

The other approach to estimating crater depths is through theory. Early, order-of-magnitude estimates were made by Whipple (58), Opik (58a), and others. Bjork (58) performed an analysis on purely hydrodynamic grounds. Computer solutions were obtained. His results are considered very indicative of true ultra-high velocity impact. In the fifth and sixth Symposiums on Hypervelocity Impact (HIS 62 and 63) he and Olshaker have considerably extended this work.

Let us now consider the variety of penetration criteria proposed, and their divergence.

Velocity Dependence

The dependence of crater depth on velocity varies strongly; for very low velocities ($v < 1$ km/sec) penetration rises as v^2. The dependence becomes weaker as v increases. It is about $v^{4/3}$ in the velocity range for conventional guns.

Above this region, a transition to a different penetration regime occurs. Well below the speed of sound the projectile strength is sufficient that it penetrates undeformed. The resulting hole is deep, with a cross-section not much larger than the projectile. Above the speed of sound, stresses are very large and the particle is fragmented. The craters begin to approach a spherical shape. Ductile prljectiles may be "plated" over the interior of the crater. The penetration depth now goes approximately as the two-third power of velocity. This, of course, is the empirical "hypervelocity" regime which gives birth to the Ames criterion. It persists to about the limit of experimental capability. There is an indication that the velocity dependence is becoming shallower near this limit.

The theoretical predictions of Bjork suggest that at high velocities crater depths will follow approximately the 1/3 power of velocity. This encourages one to hypothesize a smooth variation, as suggested by the Hermann & Jones logarithmic data correlation (Figure A-1).

Walsh and Tillotson (HIS 63), however, have proposed an alternate theoretical attack. The hydrodynamic calculation is terminated at a relatively high shock pressure. The resulting velocity field in the growing crater is referred, by scaling laws, to an empirical low velocity crater. In essence, this restores target material strength to the calculation. The result is a dependence of penetration very nearly on the two thirds power of impact velocity. In this case, an extrapolation of the Ames criterion is valid.

In Figure A-1, calculated penetrations by aluminum projectiles in soft aluminum are compared. The Ames law, the Bjork computed point, and the Hermann & Jones logarithmic correlation agree well in the empirical range of approximately 1-10 km/second. The scatter in the data well exceeds this. Below the range, the Hermann & Jones law drops off, representing penetration by undeformed projectiles. Above the range, they diverge, and the question of extrapolation is raised.

The Ames law may be said to be <u>wrong</u> above 10 km/second, since the data are dropping below it, and it is clear that "higher terms" in the approximation must be introduced. In the text, we have arbitrarily assumed a $v^{1/2}$ variation of penetration above 10 km/second (dashed line on Figure A-1). Why did we not take $v^{1/3}$, <u>or</u> the Hermann & Jones logarithmic penetration?

Firstly, why not $v^{+1/3}$? Though the data are dropping, there is no evidence yet for a 1/3 law. In the light of the Walsh & Tillotson results, there seems no need to accept a 1/3

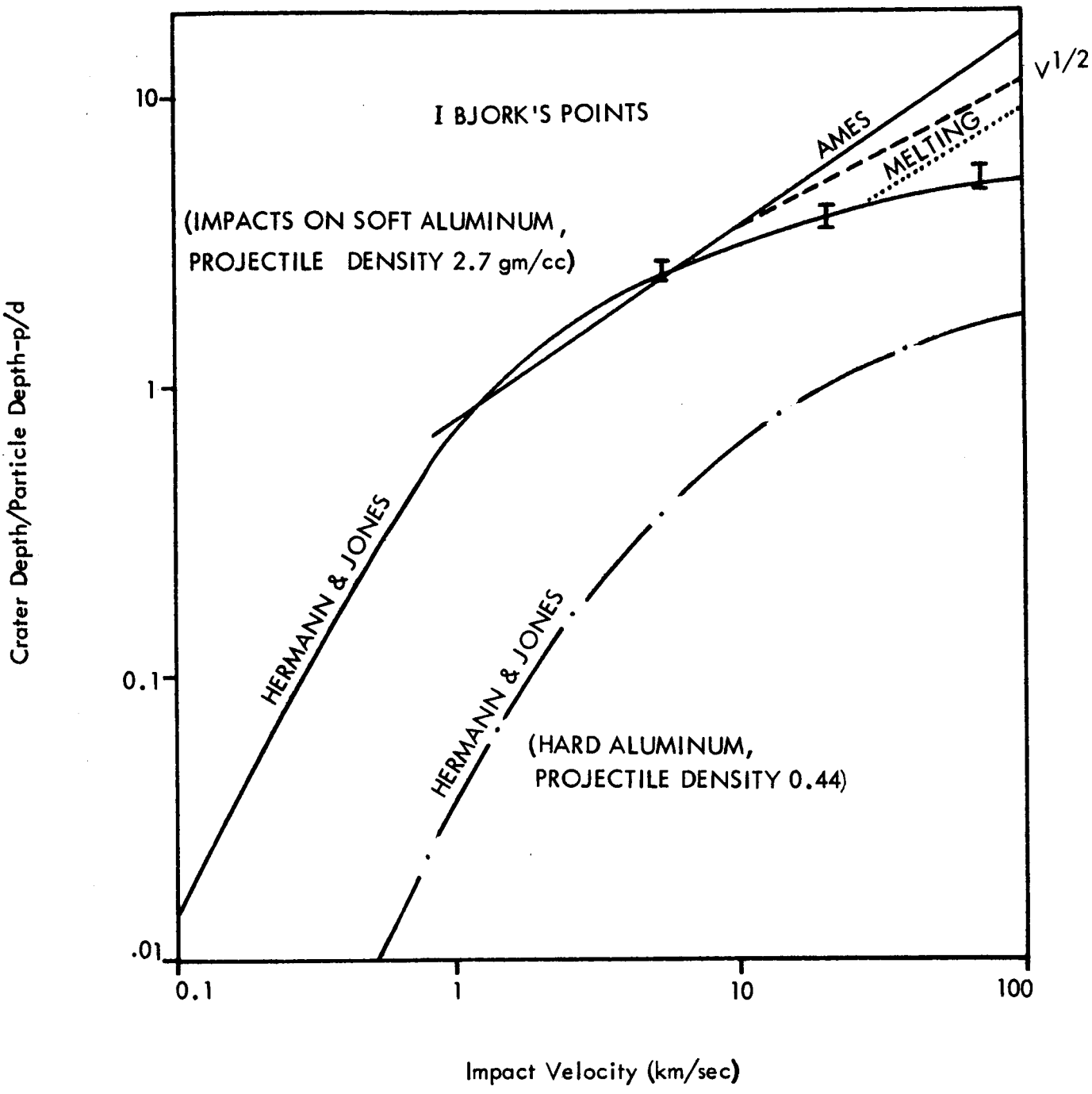

FIGURE A-1 CRATER DEPTH AGAINST IMPACT VELOCITY: VARIOUS PENETRATION CRITERIA

variation blindly. Further, Bjork (HIS 63) now suggests that impact melting of the target will cause increased penetration (dotted line in Figure A-1). A $v^{1/3}$ variation is certainly not necessary.

Secondly, why not use the Hermann & Jones logarithmic correlation (HIS 62), as does F. Whipple (63)?

Analytically, this has the form

$$\frac{p}{d} = k_1 \ln \left(1 + \frac{\rho_t v^2}{k_2 H_t} \right) \qquad \text{(A3-1)}$$

the constants k_1 and k_2 are tabulated by Hermann & Jones for various projectile-target combinations. As a two parameter relation, this fits the data better than a simple power law. There is obviously no objection to (2.1) as it stands, saving that it is a nuisance to look up logarithms to the base e.

However, this equation does not contain any particle properties. Hermann & Jones obtained a rather poor correlation of k_1 and k_2 with (ρ_p/ρ_t).

The final "data correlation" as used by Whipple is

$$\frac{p}{d} = (0.6 \pm 0.2) \left(\frac{\rho_p}{\rho_t} \right)^{2/3} \ln \left[1 + \left(\frac{\rho_p}{\rho_t} \right)^{2/3} \frac{\rho_t v^2}{(4 \pm 2) H_t} \right] \qquad \text{(A3-2)}$$

This is extraordinarily sensitive to density variation. Charters (HIS 63) indicates that for impacts on soft aluminum, the exponent of particle density drops as velocity increases. It is 2/3 at 2 or 3 km/second, and perhaps 0.55 at 6.5 km/second. Bjork and Olshaker (HIS 62) suggest (from Hugoniot studies) that this exponent is (a) a function of target material and (b) for aluminum, a function of velocity, decreasing from 0.6 to 0.55. At 5 or 6 km/second, for soft aluminum, the exponent on the Hermann & Jones correlation is about $\rho_p^{5/6}$. This is contrary to the data, and represents an accident in correlation. It certainly should not be used to predict penetration by projectiles having very low densities.

The combination of low density (0.44 gm/cc) and a stronger material (H_t increased 10x) furthermore translates the velocity transition of Figure A-1 to substantially higher

velocities. On Figure A-1, we also show a plot for 24 ST (hard) aluminum with a projectile density of (0.44). The values of k_1 and k_2 have been taken from the Hermann & Jones tabulation and scaled with ρ_p as in (2.2). Here, the $v^{1/3}$ behavior has been entirely suppressed, and the steep slope corresponding to the "undeformed projectile" is moved out to 3 or 4 km/second. Hermann & Jones clearly warn against extrapolation of their formula when the results seem physically doubtful.

APPENDIX 4

FLUX CHART DATA

1. Explorer XVI Can Data (Hastings 63, TMX 899)

Material: Beryllium Copper, Berylco #25, solution annealed to a hardness of B-60.

Puncture Rates (May 26, 1963) to 90% confidence

thickness	Punctures/sq ft day (90% conf)		mean rate	n°events	n°events
inches	upper	lower	per ft^2 dy.	May 26	July
.001"	.0393	.0224	.030	38	44
.002"	.0289	.0093	.017	10	11
.005"	.0088	.0	0	0	0

These data are transformed as follows: The thickness of equivalent aluminum is 2x that of Beryllium copper by calibration at 5 km/second. The rates are near earth, and should be multiplied by 4/3 to give an unshielded flux. We convert the thicknesses to meters of aluminum (mult by 5.08×10^{-2}) and the fluxes to m^{-2} sec^{-1}.

(mult by $4/3 \cdot \frac{1}{8.03 \times 10^3} = 1.66 \times 10^{-4}$)

Plotted Data

thickness (m)	Unshielded Puncture rate/m^2 sec	
	upper	lower
5.1×10^{-5}	6.5×10^{-6}	3.7×10^{-6}
10.2×10^{-5}	4.8×10^{-6}	1.55×10^{-6}
25.4×10^{-5}	1.46×10^{-6}	0

2. Cadmium Sulfide Cells

As yet I have only raw data for these cells, kindly communicated to me by L. Secretan. From a recent telephone conversation, I gather that we have treated the data differently. He of course has no responsibility for the way in which I have attacked the problem, which seems to me the simplest and most valid for the data avilable.

Data: The total area exposed was 40 cm^2 (Hastings (63) quotes 7.52 square inches, or 48.5 cm^2). Through February 20 (67 days or 5.8 x 10^6 seconds) the exposure was 2.3 x 10^4 m^2 sec. 10 increments in the "open area" of the cells had occurred. Increments were observed in only one cell at a time, so that it is plausible that each represents one impact. Mr. Secretan cautions that the experiment could be interrogated only irregularly, so that 10 is a lower bound.

The nominal puncture rate in 1/4 mil mylar sheet is then:

thickness (inches)	puncture rate (raw, m^{-2} sec^{-1})
.00025	4.4×10^{-4}

The conversion of thickness of mylar to equivalent aluminum is difficult. The density of mylar is 1.395 gm/cc. Neither the velocity of sound nor the Brinnell Hardness of the material (which is not available save in films) are available. Neither is there well controlled experimental data. It is known that nominally 10^{-13} kg iron particles (launched by the STL electrostatic accelerator) at 5 km/second will penetrate the quarter mil films. The experiments were not well controlled, at least in the sense that no direct comparison with aluminum was made.

Using the tensile elastic modulus (550,000 psi) one can estimate the velocity of sound as 1.4 km/second; this yields: T mylar x 3.7 = T aluminum.

Accepting the 10^{-13} kg as the mass just penetrating and using the Ames penetration equation (3.5) one obtains:

T mylar x .3 = T aluminum.

According to this, mylar has a resistance to impact comparable with an ultra strength steel.* This does not seem at all likely. Clearly the data as it stands is not very valuable. We plot T_{mylar} 3.7 = $T_{aluminum}$, indicating the uncertainty in equivalent thickness by a bar. Better calibration work should be done. With this decision, we obtain for the Cd S cells, (correnting the flux for shielding),

thickness	puncture rate
1.6×10^{-6} m	5.9×10^{-4} m^{-2} sec^{-1}

---

* At low velocities, where scaling with $(H_t)^{-1/3}$ is fairly accurate. If this calibration were correct, there would be no question but that spacecraft would be constructed exclusively of mylar film. A weight advantage of about six times would be obtained over aluminum!

3. Other Data

The remaining data are those of edition one. These were taken from Alexander, McCracken, Secretan, and Berg (1962), an excellent and complete review.

In plotting the penetration measurements, the "characteristic dimensions for penetration" must be converted to equivalent aluminum thicknesses. The choice of the Ames criterion requires, then scaling as the two-thirds root of the product of target density and velocity of sound. When more data is available, the smoothness of such a plot may be helpful in choosing a proper penetration law.

The data are listed in the Table I following. The "wires" require complete severing for an indication. They might well be assigned a smaller T.

3.1 Conversion to Equivalent Aluminum

$$T_{Al} = T \left(\frac{\rho \; c}{\rho_{Al} \; c_{Al}} \right)^{2/3} = T/A$$

Material	ρ gm/cc	c km/sec	A
Pyrex	2.8	5.6 (?)	.93
Mylar	1.4	1.4*	3.7 (see above)
Magnesium	1.7	4.6	1.5
Stainless Steel 304	7	5 (?)	.54
Copper	8.9	3.6	.58
Aluminum	2.7	5.1	-

4. Acoustic Measurements

As indicated in the text, acoustic measurements are plotted using the Ames equation in the form

$$T = (0.41) \left(\frac{p}{10^3} \right)^{1/3} \left(\frac{v \cos\theta}{10^4} \right)^{1/6} \left(\frac{P \cos\theta}{10^4} \right)^{1/3} \qquad (7.1)$$

---

* Computed from tensile elastic modulus 550,000 psi.

The mean value of ρ_p is 10^3 g/cc, of $\cos\theta$, 1/2, of v, 1.8 x 10^4 km/sec. In terms of cgs momenta, we obtain

$$T = 3.3 \times 10^{-4} \quad (p_{cgs})^{1/3}$$

The satellite measurements are summarized in the Table 2.

5. Venus Flytrap

Particles collected by the Venus Flytrap recoverable sounding rocket (Soberman et al, 63) have a cumulative size distribution varying as the - 1.3 power of particle diameter (from .2 to 3 diameter). A flux of 300 m^{-2} sec^{-1} of particles exceeding 3 in diameter is found. This is a lower bound, based on the assumption that the particles were falling with terminal velocity.

Three large holes (certainly low velocity impact) were observed in 6 micron mylar film, with an exposure of 56.6 m^2 sec.

TABLE 1

PENETRATION MEASUREMENTS

Space Craft	Material	Penetration	Equivalent Aluminum*	Exposure	Impacts	Flux
Vanguard III	pyrex	$3\ 10^{-4}$	$3.2\ 10^{-4}$	7 10	0	$1.4\ 10^{-2}$
	pyrex	$3\ 10^{-4}$	$3.2\ 10^{-4}$	$1.4\ 10^{2}$	0	$7\ 10^{-3}$
	mylar	$6\ 10^{-6}$	$1.6\ 10^{-6}$	8.7 10	0	$1.1\ 10^{-2}$
	magnesium	$6.5\ 10^{-4}$	$4.3\ 10^{-4}$	$7.2\ 10^{5}$	0	$1.4\ 10^{-6}$
Explorer VII	mylar	$6\ 10^{-6}$	$1.6\ 10^{-6}$	3.9 10	1	$2.5\ 10^{-2}$
Explorer XIII	stainless	$7.5\ 10^{-5}$	$1.4\ 10^{-4}$	$3.4\ 10^{4}$	0	$3\ 10^{-5}$
	stainless	$1.5\ 10^{-4}$	$2.8\ 10^{-4}$	$8.5\ 10^{3}$	0	$1.2\ 10^{-4}$
	"wire" Cu & enamel	$7.5\ 10^{-5}$	$1.3\ 10^{-4}$	$1.7\ 10^{3}$	0	$6\ 10^{-4}$
	"wire" Cu & enamel	$5\ 10^{-5}$	$8.6\ 10^{-5}$	$7.7\ 10^{2}$	0	$1.3\ 10^{-3}$
Explorer I	"wire" Cu & enamel	$1.7\ 10^{-5}$	$3\ 10^{-5}$	$3.6\ 10^{3}$	0	$2.8\ 10^{-4}$
Explorer II	"wire" Cu & enamel	$1.7\ 10^{-5}$	$3\ 10^{-5}$	$2.4\ 10^{2}$	2	$8.3\ 10^{-3}$
Midas II	"wire" Cu & enamel	$2.0\ 10^{-5}$	$3.5\ 10^{-5}$	$2\ 10^{3}$	0	$5\ 10^{-4}$
Samos II	"wire" Cu & enamel	$2\ 10^{-5}$	$3.5\ 10^{-5}$	$1.1\ 10^{4}$	8	$7\ 10^{-4}$
Venus Flytrap	mylar	$6\ 10^{-6}$	$1.6\ 10^{-6}$	5.7 10	3	$5\ 10^{-2}$
		meters	meters	m^2 sec		$m^{-2}\ sec^{-1}$

* See text.

TABLE 2

ACOUSTIC MEASUREMENTS

Spacecraft	Sensitivity P, dyne-sec	Observed Flux ($m^{-2}sec^{-1}$)	Penetration Inferred (m)
Explorer VIII	$2.5\ 10^{-3}$	$1.5\ 10^{-2}$	$4.4\ 10^{-5}$
	$2.5\ 10^{-2}$	$3.1\ 10^{-4}$	$1.0\ 10^{-4}$
	$2.5\ 10^{-1}$	$5.6\ 10^{-6}$	$2.1\ 10^{-4}$
		less than 2 impacts	
Vanguard III	10^{-2}	$1.3\ 10^{-3}$	$7.1\ 10^{-5}$
Pioneer I	$1.5\ 10^{-4}$	$4\ 10^{-3}$	$1.7\ 10^{-5}$
Explorer I	$2.5\ 10^{-3}$	$8.4\ 10^{-3}$	$4.4\ 10^{-5}$
Ranger I	$3\ 10^{-5}$	7.3	$1.0\ 10^{-5}$
Midas II	$3\ 10^{-4}$	$2.5\ 10^{-1}$	$2.2\ 10^{-5}$
Samos II	$3\ 10^{-4}$	$3.4\ 10^{-1}$	$2.2\ 10^{-5}$
SLV	$9\ 10^{-3}$	$1.3\ 10^{-2}$	$6.9\ 10^{-5}$
		Additional	
Venus Fly Trap		(see text of Appendix 4)	

APPENDIX 5

THE PROPERTIES OF VISUAL METEORS

This appendix briefly summarizes the relation between "visible magnitude" and the meteoroid properties of interest, i.e., mass, velocity, and structure. Some preliminary results on simulated meteors will be discussed.

Complete accounts of the theory occur in Opik (58), Levin (56), and throughout the papers of the Harvard Group. Our purpose is not to present a rigorous and complete treatment, but rather to define the problem enough so that the theory and experiment can be compared.

Briefly, it appears that the theoretical treatments are in excellent accord with the facts as far as simulated solid meteors are concerned. Since the nature and composition of dustballs are unknown, there will probably be uncertainty about them for some time.

Magnitude Scales; Photometry

The magnitude scale is very old. Ptolemy's star catalog ranks stars in six "magnitudes" in diminishing order of brightness. In modern times, the scale has been made quantitative and extended in both directions, defining magnitudes above the sixth for stars visible only in the telescope and negative magnitudes for the more brilliant objects (the visual magnitude of the sun is -26.7). Alternate scales (photographic, etc.) are defined for sensors other than the human eye. These scales are made to agree for sources of one spectral type (as, A_o stars, for photographic and visual scales). For this article, we standardize on a conventional photometric scale. (Handbook of Geophysics 1961).

A numerical expression for the "visual astronomical magnitude," M, of a source is

$$M = 2.5 \log e_o/e \qquad \text{(A5-1)}$$

Magnitude is a measure of the "illuminance," e, of the source, measured in foot candles or lux (meter candles). The constant e_o is the illuminance of a zero magnitude star, 1.944×10^{-7} foot candles or 2.094×10^{-6} lux.

Absolute Visual Magnitude of Meteors

To remove the effects of range and absorption, visual magnitudes are corrected to absolute visual magnitudes. That is, magnitudes are corrected to the value they would have if the meteor were directly overhead at an altitude of 100 kilometers. In this case, the absorption amounts to about 20% of the source flux.

Total Source Flux

If the illuminance at the surface of the earth is e, the total luminous flux Φ, at the source is

$$\Phi = (4\pi R^2 e) \frac{1}{1-\alpha} \qquad \text{(A5-2)}$$

where R is the range and α the absorption.

Alternately, we may write

$$\Phi = 4\pi R^2 e_\circ \, 10^{-0.4M} \frac{1}{1-\alpha} \qquad \text{(A5-3)}$$

$$= \Phi_\circ \, 10^{-0.4M} \qquad \text{(A5-4)}$$

where $\Phi_\circ$ is the total luminous flux from a zero magnitude meteor. At an altitude of 100 km, and with an absorption of 20%, $\Phi_\circ = 3.29 \times 10^5$ lumens.

This corresponds (685 lumens/watt) to 480 watts of monochromatic radiation of wavelength 555 millimicrons. This substantial energy production is related to the instantaneous loss of kinetic energy of the meteor via two factors, one photometric and one physical.

Relative Luminous Efficiency

The "relative luminous efficiency," γ, of any radiation source is its effectiveness in producing visual sensation relative to a source at 555 millimicrons. Typical relative luminous efficiencies are .1355 for black body radiation at 6000°K, and .016 for the iron arc.

Meteor radiation consists of line spectra arising from the decay schemes of excited atoms. The iron lines are generally predominant, other atomic species having much smaller relative efficiencies. The relative luminous efficiency of a meteor can be approximated as

$$\gamma = \gamma_{Fe} \, C_{Fe} \qquad \text{(A5-5)}$$

where C_{Fe} is the percent of iron in the meteor and $\gamma_{Fe} \sim .016$ is the relative luminous efficiency of iron radiation. Properly, equation (A5-5) should be augmented by similar terms for each element present.

Conversion of Kinetic Energy to Radiation

In addition to the above factors (photometric and chemical), the luminous flux from a meteor is reduced because not all of the meteor's kinetic energy appears as radiation.

The source of the radiant power is the instantaneous loss of kinetic energy, T

$$\dot{T} = \frac{d}{dt} \frac{1}{2} m v^2 \qquad \text{(A5-6)}$$

Of this, a fraction q appears as radiation; and, as suggested above, a fraction $q \gamma_{Fe} C_{Fe}$ is visually effective. The quantity q is a function of velocity. Opik's analysis suggests an inverse variation with velocity (1/v) for dust balls, and a direct variation (v) for heavy, compact meteoroids. The two species are equivalent near 15 kilometers per second.

Comparison of Theory and Experiment

The comparison of theories and experiment is complicated by this velocity dependence and by a difference in language among the experts.

Opik (58) tabulates (Table II) his theoretical values of the dimensionless quantity

$$\beta = q \gamma_{Fe} C_{Fe} \qquad \text{(A5-7)}$$

for both compact and dust ball cases.

R. E. McCrosky and R. K. Soberman (63) have reported results from an artificial meteor experiment. A small (2.2 gm) stainless steel pellet was accelerated by a Trail Blazer II rocket; it reentered the atmosphere with a velocity of 10 kilometers per second, and was observed by the standard two-camera technique.

In the reduction, a "luminosity coefficient" is employed which includes all of the constants mentioned above. It is assumed that $\tau = \tau_0 v$, and τ_0 is tabulated.

In our formalism, we could express the relation between kinetic energy and luminous flux as

$$\dot{T}\, q\, \gamma_{Fe}\, C_{Fe} = \mathcal{I} = \Phi_o\, 10^{-0.4M} \qquad \text{(A5-8)}$$

The Harvard Group generally uses

$$\dot{T}\, \tau_o\, v = 10^{-0.4M_{pg}} = 10^{-.72-0.4M} \qquad \text{(A5-9)}$$

where $M_{pg} = M-1.8$ is the photographic magnitude of the meteor.

Thus, to compare with Opik (A5-7), we write

$$\tau_o = \frac{q\, \gamma_{Fe}\, C_{Fe}}{\Phi_o 10^{-.72} v} = \frac{\beta}{\Phi_o\, v}\, 10^{.72} \qquad \text{(A5-10)}$$

The simulated meteor experiment yields a value

$$\tau_o = 8 \times 10^{-19} \frac{\text{(flux of zero photographic magnitude meteor)}}{\text{grams cm}^3\ \text{sec}^{-4}} \qquad \text{(A5-11)}$$

This is described as a lower limit. The expected range is (6.6-8.6). A possible correction for the chromium content of the pellet would lead to a range of (3, 10) x 10^{-19}.

We insert the value derived above for Φ_o (480 watts), obtaining

$$\frac{\beta}{v} = 7.0 \times 10^{-10} \text{ seconds/cm} \qquad \text{(A5-12)}$$

We evaluate at 15 km/sec and obtain the following experimental value, recalling that it is quoted as a lower limit and has an uncertainty something near two times associated with it.

$$\text{Iron: } \beta = 10^{-3} \qquad \text{(Experimental)} \qquad \text{(A5-13)}$$

Opik (58), in his Table II, does not distinguish between iron and stone meteoroids, i.e. no composition dependence is implied. For velocities of 14.8 km/sec the values of are as follows for the "dilute coma" and "compact coma" (comparable with McCrosky) cases:

$$\beta \text{ dilute} = 1.00 \times 10^{-3}$$

$$\beta \text{ compact} = 1.10 \times 10^{-3} \qquad \text{(Theory)} \qquad \text{(A5-14)}$$

The agreement may be mildly described as excellent.

Additional Information

A very detailed analysis of three photographic meteors has been made by Cook, Jacchia, and McCrosky (63). By careful study, they estimate the radius of an iron meteor ($0.5 \lesssim r \lesssim 0.9$ cm) and derive a mass and hence a luminosity coefficient. Choosing $r = 0.7$ cm, they obtain

$$\tau_0 = 2 \times 10^{-18} \text{ (units as above) range (1 to 6)} \qquad \text{(A5-15)}$$

or

$$\frac{\beta}{v} = 1.8 \times 10^{-9} \text{ seconds/cm}$$

$$\beta = 2.7 \times 10^{-3} \text{ at 15 km/second} \quad \text{(Experimental)} \qquad \text{(A5-16)}$$

The uncertainty here is presumably rather more than two times. The agreement is good.

Luminous Efficiency of Meteors

As noted in the text, Professor Whipple (63) flux-mass distribution has been incorporated. He utilizes a value

$$\tau_0 = 2 \times 10^{-19} \ \frac{\text{(flux of zero photographic magnitude meteor)}}{\text{grams cm}^3 \text{ sec}^{-4}}$$

as appropriate for a stony meteor. This involves some judgment as to the relative weights to be placed on (A5-11) and (A5-16), and assumes a meteoroid containing 15% iron.

This value corresponds to a zero visual magnitude stony meteor of one gram mass at velocity 30 km/second. Its uncertainty is in part experimental (perhaps 0.3 logarithmically) and in large part due to the assumption of dustball composition. Dustball compositions are unlikely to exceed 20% in iron or to be less than 1% iron; the range permits only an increase in the mass scale.

Hawkins (63) from his studies of the ionizing efficiency of radar meteors feels that the "zero magnitude mass" may be perhaps 6.5 grams. The estimate is no stronger than the last. It seems that the range of 0.5 - 5 grams is most probable. Levin (56) is often quoted as a discrepancy. He states that a 10 km/second, 1 gram, iron meteoroid is of visual magnitude 2.86.

The 0 magnitude meteoroid then has a mass of $10^{0.4 \times 2.86} =$ 11.44 grams. Since (equation 5.4) brightness $\sim mv^3$, a 30 km/second meteoroid has a mass of about 0.43 grams. For stony meteoroids, this would be up 6x or right back in the range.

Hawkins ascribes to the zero magnitude particle a mass uncertainty of 5x, which seems reasonable, although our one gram value is at the smaller end of the range. Continuation of the simulated meteor program should resolve the discrepancy between visual and ionizing efficiency, and tie down the variation of τ with velocity and composition. Since the nature of dustballs is so little understood, little direct information on these objects will be obtained.

APPENDIX 6

COMPARISON WITH F. L. WHIPPLE'S MODEL

Professor Whipple published a new meteoroid model in 1963. As we state in the text, the mass-influx relation proposed therein has been adopted as a standard by the Office of Manned Spaceflight. The penetration model for visible meteors used here (equation 6.4) and Dr. Whipple's (equation 6.8) disagree logarithmically (to the base 10) by 1.96, or 91 times. This divergence can be fairly closely accounted for in terms of our specific assumptions and his use of the Hermann & Jones Logarithmic penetration law (see Appendix 3). In the remainder of this appendix, we list the assumptions and associate with each an approximate logarithmic divergence. The sum is reasonably close to 1.96.

(a) Shielding

Whipple quotes a "near earth" flux; i.e., a spacecraft in low earth orbit is "shielded" by the earth, reducing the total influx a factor of two. This of course is a matter of choice, but the unshielded flux is more appropriate for a lunar mission.

Discrepancy: 0.3

The remainder of the discrepancy arises in the penetration law. Since the Whipple (63) flux varies as the 4.02 power of wall thickness, logarithmic deviations in wall thickness must be multiplied by this factor.

(b) Material Strength

As stated in the text, we feel that scaling penetration by the Brinnell Hardness Number of the target is not desirable for meteoroid impacts, and that certainly no power law fit to the scaling relation should be stronger than the 0.15 power of hardness. The Hermann & Jones correlation as used by Whipple is approximately equivalent to a 1/3 power scaling. Equating the Hermann & Jones and Ames criteria, our "standard aluminum" corresponds to a soft material of hardness 25 kg/mm^2. Whipple uses a standard "hard aluminum" of hardness about 123 kg/mm^2.

Discrepancy in penetration: .233 in flux: 0.936

(c) Impact Damage

We assume that the wall thickness penetrated, T, is 1.8 times the crater depth in a semi-infinite target. As stated in the text, experimental values of 2 have been observed. Whipple uses the more traditional 1.5.

Discrepancy in T: 0.079 in flux: 0.318

(d) Meteoroid Velocity

Whipple uses a mean meteoroid velocity of 22 km/sec, since his model is intended to cover the entire range of meteoroids; for the visual meteors alone, the average velocity is 30 km/sec, as used here. In both criteria, the effective exponent of velocity is about 2/3.

Discrepancy in T: +0.09 in flux: +0.362

(e) Angle of Incidence

We allow a v cos θ (normal velocity) dependence of penetration on angle of impact. This is probably too strong. Whipple does not make allowance for oblique impact. This is the one factor in which our model is less severe than Whipple's. The mean value of cos θ is a half.

Discrepancy in T: -0.20 in flux: -.804

(f) Meteoroid Density

Whipple uses a meteoroid density of 0.44 gm/cc. We feel, together with Levin and others that the derivation of this value from the deceleration equation neglects the fragmentation of the meteoroid and is fallacious. We choose one gram per cc. As used by Whipple, the Hermann & Jones equation depends on something like the 0.5 power* of the particle density, a stronger dependence than any other criterion in the (hypervelocity) literature.

Discrepancy in T: 0.178 in flux: 0.716

To summarize, we have:

		Discrepancy in flux:
(a)	shielding	0.300
(b)	material strength	0.936
(c)	impact damage	0.318
(d)	meteoroid velocity	0.362
(e)	angle of incidence	-0.804
(f)	density	0.716
	Total	1.828

* Here, we are discussing the dependence of $T/m^{1/3}$. In Appendix 3, we compared T/d, and the density dependence is higher by $\rho_p^{1/3}$.

The net remaining discrepancy, 0.13, is certainly due to our underestimating the dependence of the Hermann & Jones correlation on either density, hardness, or velocity.

Comparing the Whipple penetration model and our own on an equivalent basis, that is, both "near earth" or deep space, the divergence is 46 times. The "softest" statement in the set above is that on angle of incidence, which would make the discrepancy worse.

It should be emphasized that this discrepancy in flux corresponds to only a 2.6 times difference in penetration. Clearly, in constructing a meteoroid puncture model a very careful and conscientious analysis of the penetration law is required.

APPENDIX 7

VALUE OF THE SA-9 AND SA-8 SHOTS

The Saturn launched micrometeoroid measurement capsules have the capability to substantially reduce the size of the error envelopes shown on Figure 7. They should delimit the penetrating power of meteoroids clearly. Since the thickness (.016 inch) aluminum is small, extrapolation will still be necessary to apply this data to spacecraft design. Further, the "proof" of bumper wall structures will remain a major uncertainty.

In the following table, we summarize the exposures and thicknesses of the SA-9 experiments; for three hypothetical flux levels, we show how the results might appear. The shielding factor employed is 4/3, the same as for Explorer XVI. On Figure A-2, we plot the results for the three cases:

(a) The heavier thicknesses (.008" and .016") have no punctures. As in Figure 7, the tail of the arrow is a flux which is 95% likely to result in puncture. The slash in the middle of the arrow is a flux 50% likely to result in puncture.

(b) Hasting's least square fit of the Explorer XVI data is valid. The expected counts (in the table) show that only small error flags would be necessary.

(c) An optimistic estimate of the flux is confirmed.

It is seen that the SA-9 and SA-8 should markedly reduce the uncertainty in the significant range for astronauts. However, unless the Saturn results, like the hypothesized cases, are extreme, they should have only a modest effect in the significant range for spacecraft.

APPENDIX 8 TABLE

VALUE OF THE SA-9 AND SA-8 SHOTS

Wall Thickness			Area	Exposure (1 year)	Explorer XVI Flux	Flux For No Counts		Optimistic Flux	
						$m^{-2}sec^{-1}$			
inches	meters	log	m^2	m^2sec	counts	(50%)	(95%)	$m^{-2}sec^{-1}$	counts
.0015	$3.8x10^{-5}$	-4.4	4	$1.26x10^{7}$	72	$7.3x10^{-8}$	$3.16x10^{-7}$	$5.5x10^{-6}$	52
.008	$2.0x10^{-4}$	-3.7	16	$5.1x10^{8}$	340	$1.9x10^{-9}$	$7.8x10^{-9}$	5.10^{-7}	190
.016	$4.0x10^{-4}$	-3.4	180	$5.7x10^{9}$	1500	$1.6x10^{-10}$	$7x10^{-10}$	$4x10^{-8}$	170

Fluxes, unshielded; counts, shielded.

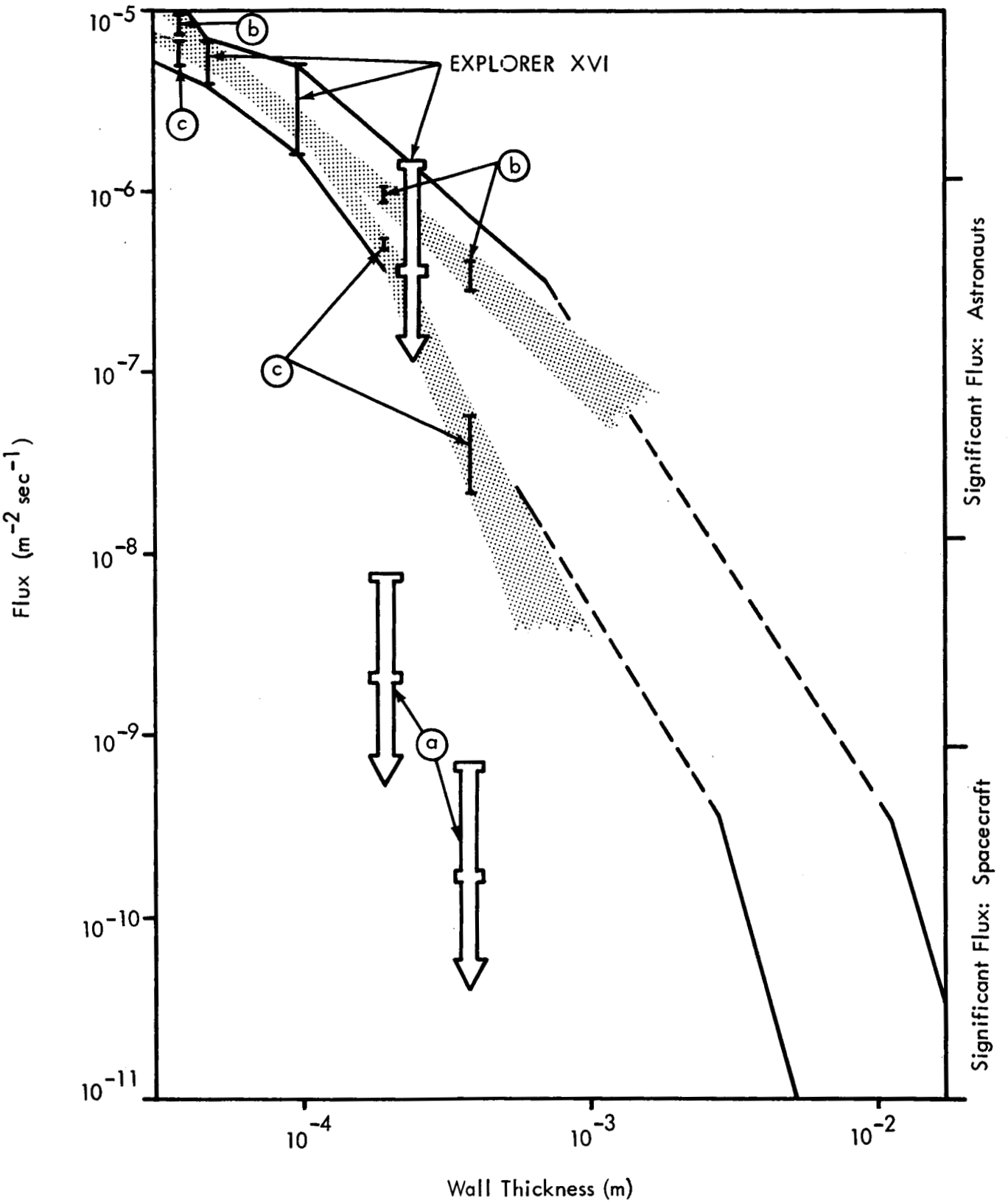

FIGURE A-2 PENETRATION FLUX ERROR ENVELOPES FOLLOWING MEASUREMENTS BY SA-9, SA-8. THREE HYPOTHESISED FLUX LEVELS, ⓐ, ⓑ, ⓒ, ARE LISTED IN THE TEXT.